

Neuroprotective Effect of Nortriptyline in Overt Hepatic Encephalopathy Through Attenuation of Mitochondrial Dysfunction

ASN Neuro
Volume 10: 1–20
© The Author(s) 2018
Article reuse guidelines:
sagepub.com/journals-permissions
DOI: 10.1177/1759091418810583
journals.sagepub.com/home/asn


Ji Heun Jeong¹, Do Kyung Kim¹, Nam-Seob Lee¹, Young-Gil Jeong¹,
Ho Won Kim², Jong-Seok Kim², and Seung-Yun Han^{1,2}

Abstract

Hyperammonemia associated with overt hepatic encephalopathy (OHE) causes excitotoxic neuronal death through activation of the cytochrome C (CytC)-mediated mitochondria-dependent apoptotic pathway. We tested the therapeutic effect of nortriptyline (NT), a mitochondrial permeability transition pore (mPTP) blocker that can possibly inhibit mitochondrial CytC efflux to the cytosol on *in vivo* and *in vitro* OHE models. After ensuring the generation of OHE rats, established by bile duct ligation (BDL), they were intraperitoneally administered either 20 mg/kg NT (i.e., BDL+NT) or another vehicle (i.e., BDL+VEH) for 14 days. Compared with the control, BDL+VEH showed an increment of motor deficits, cell death, synaptic loss, apoptosis, and mitochondria with aberrant morphology in substantia nigra compacta dopaminergic (DA-ergic) neurons. However, the extent was significantly reversed in BDL+NT. Subsequently, we studied the neuroprotective mechanism of NT using PC-12 cells, a DA-ergic cell line, which exposed glutamate used as an excitotoxin. Compared with the control, the cells exposed to 15 mM glutamate (i.e., GLU) showed incremental cell death, apoptosis, and demise in mitochondrial respiration. Importantly, efflux of CytC from mitochondria to cytosol and the dissipation of mitochondrial membrane potential ($\Delta\Psi_m$), an indicator of mPTP opening, were prominent in GLU. However, compared with the GLU, the cells cotreated with 10 μ M NT (i.e., GLU+NT) showed a significant reduction in the aforementioned phenomenon. Together, we concluded that NT can be used for OHE therapeutics, mitigating the excitotoxic death of substantia nigra compacta DA-ergic neurons via mPTP-associated mitochondrial dysfunction inhibition.

Keywords

apoptosis, glutamate excitotoxicity, hepatic encephalopathy, mitochondrial permeability transition pore, nortriptyline.

Received August 2, 2018; Received revised September 21, 2018; Accepted for publication October 1, 2018

Introduction

Hepatic encephalopathy (HE) is a continuum of neuropsychiatric abnormalities observed in patients with hepatopathy such as liver cirrhosis after exclusion of other known central nervous system (CNS) pathologies (Ferenci et al., 2002). As the current diagnosis of HE is solely dependent on psychometric tests to assess the broad spectrum of neuropsychiatric disturbances, minimal HE (MHE), the earliest form of HE, is sometimes difficult to diagnose and thus delay the applications of laxatives, a first-line therapy for lowering the ammonia (NH₃) burden (Manning and Delp, 1958; Nabi and Bajaj, 2014). In that case, MHE, which is initially reversible in nature, is likely to be converted to overt HE (OHE),

which is difficult to cure and thus strongly associated with increased rates of hospitalization and mortality (Romero-Gómez et al., 2015). For these reasons, preclinical research to reveal the diagnostic modalities that possess high accuracy at the early stage of HE (i.e., MHE) or

¹Department of Anatomy, College of Medicine, Konyang University, Daejeon, South Korea

²Myunggok Medical Research Institute, College of Medicine, Konyang University, Daejeon, South Korea

Corresponding Author:

Seung-Yun Han, Department of Anatomy, College of Medicine, Konyang University, Daejeon 35365, South Korea.

Email: jjzy@konyang.ac.kr



adversely, the therapeutic strategies that can act on even the late stage (i.e., OHE) are urgently needed.

Among the multifaceted pathophysiology that underlies HE, hyperammonemia-induced astrocyte dysfunction is the best-characterized hypothesis (Norenberg, 1998; Brusilow et al., 2010). In healthy people, nitrogenous compounds such as proteins are metabolized into NH_3 by gut microflora and transported to the liver, where it is converted to urea, which is readily excreted by urine (Watford, 2003). In case of hyperammonemia in patients with certain hepatopathy, CNS astrocytes become exposed to excessive NH_3 , and these are converted to hyperosmolar glutamine, which contributes to the swelling and consequent dysfunction of host astrocytes (Norenberg, 1987; Rao and Norenberg, 2014). Thus, the resulting impairment of their ability to take up glutamate from the extraneuronal space, one of the primary roles of astrocytes, can eventually cause the glutamate-induced excitotoxicity (GE) onto nearby neurons.

Once initiated, GE results in mitochondria-dependent apoptosis cascade in neurons. In brief, cytosolic calcium overload triggered by GE opens the mitochondrial permeability transition pore (mPTP), a protein complex located in the mitochondrial inner membrane, and via this opening, cytochrome C (CytC) translocates from the mitochondrial matrix to the cytosol. Afterward, the cytosolic CytC forms the apoptosome, and eventually, the downstream caspase-3 is activated and thereby leads to DNA damage (Jiang and Wang, 2000). Furthermore, apart from the role in CytC translocation, the mPTP opening can disrupt the proton gradient, which in turn mediates the concurrent dissipation of mitochondrial membrane potential ($\Delta\Psi_m$; Precht et al., 2005). The mitochondrial events described earlier are believed to mediate the mitochondrial dysfunction and eventual demise of the host neuron in various CNS pathologies associated with OHE (Lax et al., 2017; Niknahad et al., 2017). In this regard, the pharmacological means to interfere one or more steps in these cascades can offer the opportunity to retard or even stop the progression of OHE; however, the therapeutic potential of the pharmacological inhibition of the opening of mPTP on HE must be further investigated.

As described earlier, owing to the urgent need to search for agents with a neuroprotective potential on OHE, in this study, we selected a target drug within the CNS-acting medicinal library that are readily available in the clinical field. Among the possible drugs, nortriptyline (NT), a tricyclic antidepressant currently used in clinical settings, was recently reported to possess the blocking property on mPTP in both isolated liver and brain mitochondria (Zhang et al., 2008). Furthermore, a recent work demonstrated that NT was protective in two models of chronic neurodegeneration, namely,

amyotrophic lateral sclerosis and Huntington disease (Wang et al., 2007).

Considering its clinical availability together with its mPTP-blocking property on mPTP, in this study, NT was selected as the target drug and tested for its possible therapeutic effect on experimental OHE *in vivo* and *in vitro*. Notably, owing to the highly susceptible nature of HE, dopaminergic (DA-ergic) neurons in the substantia nigra compacta (SNc) were selected as the *in vivo* target region for the possible protection of NT. On the other hand, given the well-known role of GE on HE-associated neurotoxicity, a glutamate challenge on PC-12 cells, a rat pheochromocytoma cell line that is widely accepted as DA-ergic, was used as an *in vitro* model of OHE.

Materials and Methods

Reagents and Chemicals

RPMI-1640 medium, fetal bovine serum, phosphate buffer solution (PBS), and a penicillin/streptomycin mixture were obtained from Thermo Scientific (HyClone, South Logan, UT). L-glutamic acid, formalin, and paraformaldehyde (PFA) were obtained from Junsei (Tokyo, Japan). NT, Hoechst 33258, dimethylsulfoxide, 3-(4,5-dimethyl-2-thiazolyl)-2,5-diphenyltetrazolium bromide (MTT), cyclosporin A, sodium cacodylate, glutaraldehyde, toluidine-blue, epoxy resin, and lead(II) citrate were purchased from Sigma-Aldrich (St. Louis, MO). The Muse Annexin V-FITC/PI (propidium iodide) Apoptosis Detection Kit and Muse Mitopotential Kit were from Merck (Kenilworth, NJ). Slides for automated enzyme-linked immunosorbent assay (ELISA) to measure total bilirubin (TBIL-P), direct bilirubin (DBIL-P), aspartate aminotransferase (AST-P), alanine aminotransferase (ALT-P), albumin (ALB-P), and NH_3 (NH_3 -P) levels were from Fujifilm (Tokyo, Japan). Isoflurane (Vetflurane) and pentobarbital sodium (Euthasol) were from Virbac (Fort Worth, TX). Rabbit anti-CytC (Cat# 11940 RRID:AB_2637071) and rabbit antiglyceraldehyde-3-phosphate dehydrogenase (GAPDH; Cat# 2118 RRID:AB_561053) were from Cell Signaling Technology (Beverly, MA). Rabbit anti-tyrosine hydroxylase (TH; Cat# ab112 RRID: AB_297840) and mouse anti-isocitrate dehydrogenase 2 (IDH2; Cat# ab55271 RRID: AB_943793) were from Abcam (Cambridge, UK). The rabbit anti-gial fibrillary acidic protein (GFAP; Cat# PA1-10019 RRID: AB_1074611) was obtained from Thermo Scientific. DeadEnd Colorimetric terminal deoxynucleotidyl transferase dUTP nick-end labeling (TUNEL) assay kit was from Promega (Madison, WI). Seahorse XF Cell Mito Stress Test Kit were from Agilent (Santa Clara, CA). The horseradish peroxidase-conjugated antirabbit IgG,

the biotinylated antirabbit or antimouse IgG, VECTASTAIN[®]-Elite avidin-biotin complex, and 3,3'-diaminobenzidine tetrahydrochloride (DAB) were purchased from Vector Laboratories (Burlingame, CA). Mitochondria/Cytosol Fractionation Kit was from Merck (Kenilworth, NJ). All other chemicals and reagents were of analytical grade.

Bile Duct Ligation and Drug Administration

The animal protocol used in this study was reviewed and approved on the basis of the ethical procedures and scientific care by the Institutional Animal Care and Use Committee in Konyang University (Daejeon, Korea). All experimental procedures were performed in accordance with the National Institutes of Health (Bethesda, MD) Guidelines for the Care and Use of Laboratory Animals, Eighth Edition (National Research Council, 2010). Forty-four male Sprague-Dawley rats (weight, 220–250 g; age, 7 weeks) were purchased from Harlan (Indianapolis, IN; RRID:RGD_737903). After arrival, the rats were stabilized for 7 days, with access to water and food *ad libitum* at a constant temperature (22°C ± 2°C) and humidity (40%–60%) with a 12-hr light/dark cycle. After then, the rats were randomly divided into two experimental groups, namely, the SHAM ($n=16$) and bile duct ligation (BDL) group ($n=28$). For the rats in the SHAM group, a horizontal laparotomy was made, and then the abdominal wall was

immediately closed without ligation of the common bile duct. For the rats of the BDL group, after a horizontal laparotomy, the common bile duct was double-ligated using 4-0 silk sutures, and then the abdominal wall was closed. Surgeries were performed under inhalation anesthesia at 1.5% isoflurane in a combination of oxygen and nitrous oxide (30:70). The operated rats were returned to their home cage and allowed access to water and food *ad libitum* at a constant temperature and humidity until their sacrifice. On postoperative day (POD) 14, four rats randomly selected from each group were sacrificed to confirm the successful establishment of rats with hepatopathy. The remaining rats in the BDL group ($n=24$) were further divided into two groups ($n=12$ per group), namely, the BDL+VEH and BDL+NT groups. For each rat in the BDL+VEH group, 200 μ l of normal saline used as vehicle (VEH) was daily administered via an intraperitoneal (i.p.) route for an additional 14 days. On the other hand, for the BDL+NT group, NT was dissolved in equal amounts of normal saline to a concentration of 20 mg/kg and i.p. administered daily for the same duration. Immediately after the last course of treatment in the 14-day administration period (i.e., at POD 28), the rats in the SHAM, BDL+VEH, and BDL+NT groups ($n=12$ per group) were all sacrificed, and their brains were harvested. The schedule of the *in vivo* experiment is summarized in Figure 1(a).

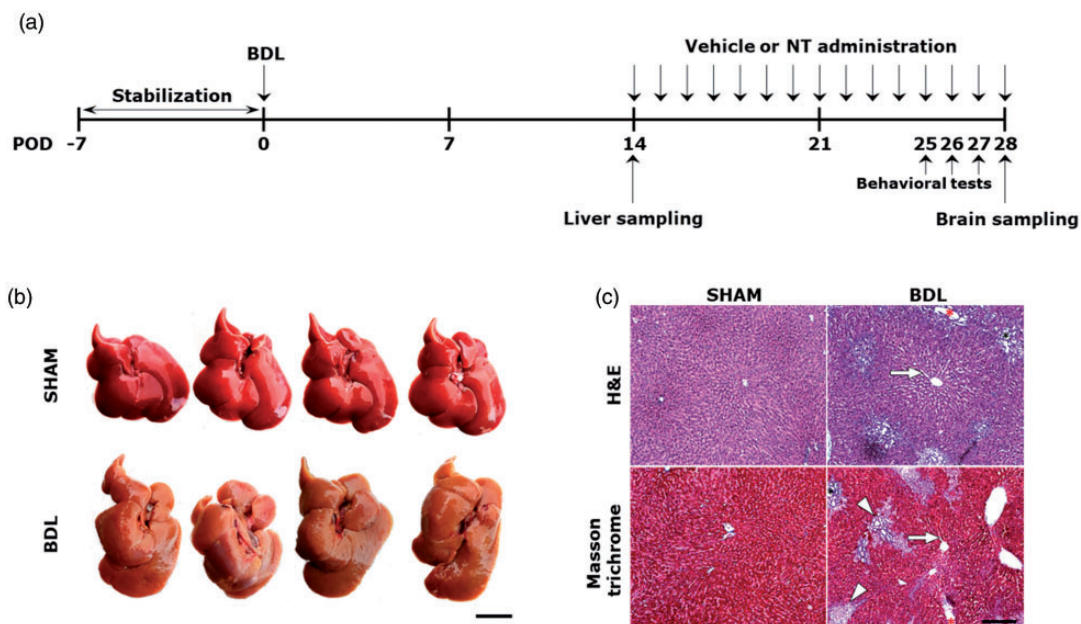


Figure 1. Establishment of liver cirrhosis-like hepatopathy in the BDL group at POD 14. (a) The *in vivo* experimental protocols in this study. (b) Macroscopic image of the livers of SHAM and BDL groups. Cirrhotic changes with rough and yellowish surface are shown in livers of the BDL group. Scale bar = 2 cm. (c) H&E and Masson trichrome-stained images of livers of SHAM and BDL groups ($n=4$ per group). Widened sinusoids, bile duct distention, and fibrotic areas are depicted with white arrows, red asterisk, and white arrowheads, respectively. Scale bar = 200 μ m. BDL = bile duct ligation; POD = postoperative day; NT = nortriptyline; H&E = hematoxylin and eosin.

Tissue Sampling

All the rats were sacrificed using an overdose of pentobarbital sodium (100 mg/kg, i.p.). On POD 14, to confirm the establishment of hepatopathy, blood and livers were harvested from the rats randomly selected from the SHAM and BDL groups ($n=4$ per group). Blood samples were transferred to evacuated tubes containing heparin solution as anticoagulant and then centrifuged at $3,000\times g$ for 10 min to yield the serum. Livers were rapidly excised and photographed, and the left lateral lobe was selectively cut and fixed with 10% neutrally buffered formalin (NBF). The obtained sera, liver photographs, and NBF-fixed livers were utilized for future works, including liver function test, gross inspection, and histopathological examination, respectively. On POD 28, the rats in the SHAM, BDL+VEH, and BDL+NT groups ($n=12$ per group) were transcatheterially perfused with 4% PFA under the anesthesia induced by pentobarbital sodium (50 mg/kg, i.p.), and their brains were obtained. Post fixation, the brains were immersed in 4% PFA or 1.5% glutaraldehyde at 4°C for 24 hr and further subjected to tissue processing steps for either light microscopy ($n=8$ per group) or transmission electron microscopy (TEM, $n=4$ per group), respectively.

Liver Function Test

After the collection of sera with the procedures described earlier, they were stored at -70°C until assayed. The levels of serum TBIL, DBIL, AST, ALT, ALB, and NH_3 were assayed using the commercial ELISA slides, namely, TBIL-P, DBIL-P, AST-P, ALT-P, ALB-P, and NH_3 -P, respectively. Each of the resulting absorbance was detected using the corresponding automatic ELISA machine (DRI-CHEM 3000, Fujifilm) in accordance with the manufacturer's instructions.

Histopathological Examination

The 10% NBF-fixed livers and 4% PFA-fixed brains were dehydrated with an ethanol gradient series, embedded in paraffin, and sliced into 5- μm sections using a microtome (RM2255, Leica, Nussloch, Germany). For the livers from the SHAM and BDL groups ($n=4$ per group), histopathological changes induced by BDL were examined using hematoxylin and eosin (H&E) and Masson's trichrome stain. Both stains were performed according to previous studies (Fischer et al., 2008; Krishna, 2013; Gil et al., 2016). For assessment of the degree of fibrosis, the Knodell histology activity index (HAI) was slightly modified and utilized (Brunt, 2000). The following criteria were used in this study: 0 = no fibrosis; 1 = fibrous expansion of some portal tract with or without short fibrous septa; 2 = fibrous expansion of most portal tracts with or without fibrous septa; 3 = fibrous

expansion of the portal tract with occasional portal-to-portal bridging; 4 = fibrous expansion of portal tracts with marked portal-to-portal and portal-to-central bridging; and 5 = marked bridging (portal to portal or portal to central) with occasional nodules. For the brains from the SHAM, BDL+VEH, and BDL+NT groups ($n=8$ per group), the number of SNc DA-ergic neurons was examined using cresyl-violet staining as previously described (Alvarez-Buylla et al., 1990). Each of the two microscopic fields of the liver and SNc-contained brain sections randomly selected from a collection of serial sections of individual rats and then photographed at $\times 200$ and $\times 400$ magnification by digital camera connected with light microscope (DM4, Leica Microsystems GmbH, Wetzlar, Germany). By using these images, the SNc neurons were counted and averaged per high-power fields (HPFs; $\times 400$) and then per group. At that time, only the soma with visible nucleoli was regarded as an intact neuron.

Behavioral Tests

The three different behavior tests were subjected to all the groups ($n=12$ per group) at different time points between POD 25 and 27. Before each behavior test, the rats were placed in the testing room (total area of 4.8 m^2) for 30 min to allow habituation with the test environment and observers. The intertask intervals were 24 hr, and all the behavioral tests were performed between 9:00 a.m. and 4:00 p.m. The order of tests was as follows: open-field test (OFT), rotarod test, and Y-maze test, each executed on PODs 25, 26, and 27, respectively. All individual tests were triplicated, and the resulting data were averaged per rat and then per group. For normally distributed data, we compared means between the groups by using a one-way analysis of variance and post hoc test.

Open-Field Test

Spontaneous locomotor activity was evaluated using the OFT as previously described (Carter and Shieh, 2015; Tatem et al., 2014). The OFT apparatus consists of a square Plexiglas cage (72 \times 72 \times 30 cm) with walls to minimize exposure to light and noise. The rats were individually placed at the bottom of the OFT apparatus and allowed to move freely during a 10-min duration. The measured horizontal activity, including the distance moved (cm) and velocity (cm/s), were scored and recorded automatically over the course of 10 min by using a video-tracking system connected to a computer equipped with the Ethovision XT 7.0 software (Noldus, Wageningen, the Netherlands; RRID:SCR_000441). To assess the vertical activity (i.e., rearing behavior), the total number of rearing over the course of 10 min was scored with the aids of a handheld motion picture camera

(EOS 100D; Canon, Tokyo, Japan). After behavioral monitoring, the floor was cleaned with 70% ethanol solution and left to dry before testing the next animal.

Rotarod Test

Motor coordination was evaluated using the rotarod test as previously described (Shiotsuki et al., 2010). We placed the rats on a rotating rod (7 cm in diameter) in the rotarod apparatus (Ugo Basile Biological Research Apparatus, Varese, Italy) and recorded the time (s) of latency to fall from the rod. The velocity of the rotation of the rod was accelerated from 4 to 40 rpm over a 5-min period. When the rats fell off the rod, the trial ended. Rats that remained on the rod for >5 min were given a maximum score of 300 s.

Y-Maze Test

Spatial working memory and spontaneous locomotor activity were evaluated using the Y-maze test as previously described (Conrad et al., 1996). The maze consists of three identical arms (50 cm in length, 20 cm in height, and 10 cm in diameter) labeled with A, B, or C, respectively, diverging at 120° angles from a central point. Each rat was placed in the center of the arm and allowed to move freely for 8 min without any hindrance or stimulation. The sequence of the arm entries was manually recorded. The rats were considered to have entered the arm when all four paws were over half the length of the runway. Alternation rate was defined as entries into all three arms on consecutive occasions by using the following formula: alternation rate (%) = number of alternations / (number of total arm entries - 2) × 100. The experiments were performed in a dimly illuminated dark room. After each rat was tested, the wall and floor of the maze were cleaned using 70% alcohol.

Immunohistochemistry

Two slices each contains the SNc, and the striata were randomly selected per collection of serial sections of individual rats ($n=8$ per group). The brain slices containing the SNc or striatum were deparaffinized in xylene, hydrated by a decreasing ethanol gradient series, and washed twice in distilled water. For immunohistochemistry, while SNc-contained slices were incubated with rabbit anti-TH, the striatum-contained slices were incubated with rabbit anti-GFAP, both of which were diluted in PBS to 1:200, in a humid chamber for 24 hr at 4°C. After three washes in PBS, each of the slices was incubated with secondary antibody solutions containing biotinylated antirabbit IgGs (Vector Laboratories), diluted in PBS at a concentration of 1:250 for 2 hr at 23°C. After three washes in PBS, the slides were further incubated with a VECTASTAIN-Elite avidin-biotin complex Kit

for 1 hr at 23°C. The resulting immunoreactivities (IRs) turned to dark-brown color after the addition of DAB, a chromogen. After mounting, five of the randomly selected slices were photographed using a digital camera connected to a DM4 light microscope for examinations of SNc TH-IRs (×630), striatal TH-IRs (×50), or SNc GFAP-IR (×400), respectively. In each photograph, the averaged relative optical intensities of GFAP- or TH-IR per HPF and then per group were calculated with the aid of Image J (v1.49, National Institutes of Health). Final data were expressed as percentages (%) of the control.

Terminal Deoxynucleotidyl Transferase dUTP Nick-End Labeling Assay

To assess SNc neuronal apoptosis, the TUNEL assay was used. Two slices containing SNc were randomly selected per rat ($n=8$ per group), deparaffinized, and hydrated. The apoptotic SNc neurons were labeled using a commercial kit in accordance with the manufacturer's protocol. After the visualization of the TUNEL-positive reactions by the addition of DAB used as a chromogen, the slices were mounted and five of the randomly selected HPFs were photographed at ×400 magnification. Three blind observers counted the number of TUNEL-positive cells/HPF, and the numbers were averaged per group. In each photograph, TUNEL reactivities were classified into three categories as follows: TUNEL⁺ (low), TUNEL⁺⁺ (moderate), and TUNEL⁺⁺⁺ (high). Only the TUNEL⁺⁺⁺ neurons were considered as TUNEL-positive.

Transmission Electron Microscopy

The mitochondrial ultrastructure was observed on TEM as previously described (Graham and Orenstein, 2007). The 1.5% glutaraldehyde-fixed brains from the SHAM, BDL+VEH, and BDL+NT groups ($n=4$ per group) were sliced into 50-μm sections by using a vibratome (VT1200S, Leica). With the aids of the toluidine-blue stain, the SNc-containing tissue cubic samples (1 mm × 1 mm × 50 μm) were selectively cut. The cubic sample was immersed in 1% osmium tetroxide diluted in 0.1 M cacodylate buffer and embedded in an epoxy resin. The ultrathin sections (50 nm) of the SNc region were obtained using the EM UC7 ultramicrotome (Leica). After staining with 3% lead(II) citrate, the sections were examined using TEM (HT7700; Hitachi, Tokyo, Japan). At that time, the SNc neurons were discriminated from adjacent glial cell components on the basis of the morphological characteristics of typical neurons, and then their mitochondria were selectively photographed.

Cell Culture

PC-12 cells were obtained from the Korean Cell Line Bank (Seoul, Korea; RRID:CVCL_0481). PC-12 cells were seeded in 25 cm² polystyrene flasks with RPMI-1640 medium containing 10% heat-inactivated fetal bovine serum, 100 U/ml penicillin and 100 µg/ml streptomycin. Cells were incubated at 37°C under a humidified atmosphere of 95% air and 5% CO₂. The culture medium was replaced every 48 hr, and cultures were split at a ratio of 1:3 twice a week. Before the experiments, cell viability was checked using the trypan-blue dye exclusion test, and only cell batches that showed up to 95% viability were used.

Cell Viability Assay

To study the protective effect of NT on GE-induced neurotoxicity and to optimize the appropriate dosages of glutamate and NT for studying upstream mechanisms, cell viability was evaluated with the MTT assay as previously described (Stockert et al., 2012). For this, cells were seeded in 96-well plates at a density of 1×10^4 cells/well. The stock solutions of glutamate (100 mM in RPMI-1640 without serum) and NT (1 mM in PBS) were diluted in the culture medium immediately before addition to each well to yield the desired final concentrations. To estimate the median lethal dose (LD₅₀) of glutamate and the maximum allowable concentration (MAC) of NT, PC-12 cells were treated with different concentrations of glutamate (0, 1, 5, 10, 15, and 20 mM) or NT (0, 2.5, 5, 10, 50, and 100 µM) for 24 hr ($n = 8$ wells per concentration). Then, the cells were incubated with 10 µl of MTT solution (diluted in PBS to a concentration of 5 mg/ml) per well for 3 hr at 37°C. After the removal of the culture medium, the remaining insoluble dark-blue formazan crystals were lysed with 100 µl of dimethylsulfoxide per well. The absorbance was measured at 570 nm in an ELx800UV microplate reader (Bio-tek Instruments, Winooski, VT) and averaged per concentration. For an easier comparison, the data were expressed as percentages of the untreated controls.

Cell Treatment Protocol

After identifying 15 mM as the LD₅₀ of glutamate and 10 µM as the MAC of NT by cell viability assays (Figure 5(a) and (b)), the concentrations were selected as the optimal doses for all the following *in vitro* studies. For an easier description, while the PC-12 cell group treated with 15 mM glutamate will be referred to as “GLU,” the cell group treated with 15 mM glutamate and concomitant addition of 10 µM NT will be referred to as “GLU+NT” hereinafter.

Hoechst 33258 Stain

From among the methods to quantify apoptosis, we selected cellular staining with Hoechst 33258, a blue nucleus marker. For this, PC-12 cells were seeded in 12-well plates at a density of 1×10^5 cells per well, where the sterilized 12 Ø coverslip was located at the bottom. The GLU– and GLU+NT groups were prepared as described earlier ($n = 4$ coverslips per group). After 12 hr of incubation, all groups were fixed with 4% PFA. After three washes, the coverslips were incubated with 500 µl of Hoechst 33258 solution (1 mg/ml in H₂O) at 23°C for 15 min. After three washes, coverslips were mounted on slides and observed under a laser confocal microscope (LSM-700; Carl Zeiss, Oberkochen, Germany). The shrunken nuclei, a signature of ongoing apoptotic nucleus, were counted in the captured images of five HPFs that were randomly selected from each coverslip and averaged per group.

Flow Cytometry for Apoptosis and $\Delta\Psi_m$ Measurement

To quantify the apoptosis and the $\Delta\Psi_m$ of the PC-12 cells in response to the different treatments, Muse Cell Analyzer (Merck), an automated fluorescence-activated cell sorting device, and the corresponding assay kits (i.e., Annexin V-FITC/PI Apoptosis Detection Kit and Mitopotential Kit) were employed. The Annexin V-FITC/PI Apoptosis Detection Assay Kit utilizes a fluorescein isothiocyanate (FITC) conjugated to Annexin-V as an apoptotic cell marker and PI as a dead cells marker. On the other hand, the MitoPotential Assay Kit utilizes a cationic, lipophilic MitoPotential dye (unidentified) as a detection marker of changes in the $\Delta\Psi_m$ and 7-aminoactinomycin D as an indicator of cell death. For both experiments, cells were seeded in 12-well plates at a density of 1×10^5 cells/well, and the GLU– and GLU+NT groups were prepared as described earlier ($n = 4$ wells per group). After 12 hr of incubation, the changes in apoptosis and $\Delta\Psi_m$ were measured in accordance with the manufacturer's indications. The obtained results from the Annexin V-FITC/PI Apoptosis Detection Assay Kit represented a percentage of live cells, early/late apoptotic cells, and dead cells. On the other hand, those from the MitoPotential assay represented a percentage of live cells with intact/depolarized $\Delta\Psi_m$ and dead cells with intact/depolarized $\Delta\Psi_m$.

Mitochondrial Oxygen Consumption Rate Measurement

To evaluate the mitochondrial bioenergetics of PC-12 cells in response to the different treatments, the mitochondrial oxygen consumption rate (OCR) was assessed using the XF24 Extracellular Flux Analyzer (Agilent).

In detail, the cells were seeded at a density of 5×10^4 cells/well in XF24 cell culture microplates (Seahorse Bioscience) and cultured for 24 hr to obtain a homogeneous monolayer. At 12 hr after preparation of the control, GLU, and GLU+NT groups with the method described earlier ($n=3$ wells per group), for equilibration, all the mediums were substituted with the serum-free RPMI-1640 medium supplemented with 25 mM glucose, 1 mM pyruvate, and 2 mM glutamine and further incubated at 37°C in a CO₂-free incubator for 1 hr prior to the experiment. A calibration cartridge (Seahorse Bioscience) was equilibrated for 2 hr. Afterward, ports A, B, and C were loaded with mitochondrial uncouplers included in Seahorse XF Cell Mito Stress Test Kit (Agilent; i.e., 10 μM oligomycin A, 3 μM carbonyl cyanide-4-(trifluoromethoxy)phenylhydrazone [FCCP], and 10 μM rotenone + 10 μM antimycin A, respectively). All the uncouplers were diluted in XF assay medium to achieve the target concentrations. This allowed for an estimation of the contribution of individual parameters for basal respiration, ATP production, proton leak, and maximum respiration. All the OCRs were normalized by the number of viable cells at the end of each experiment.

Multicolor Immunofluorescence

To quantify the efflux of CytC from the mitochondria to cytosol in PC-12 cells, followed by the different treatments, multicolor immunofluorescence staining was performed. For this, the PC-12 cells were seeded in 12-well plates at a density of 1×10^5 cells per well, where the sterilized 12 Ø coverslip was located at the bottom and the GLU- and GLU+NT groups were prepared as described earlier ($n=4$ coverslips per group). After 12 hr of incubation, all coverslips were fixed with 4% PFA for 1 hr, permeabilized with 0.25% Triton X-100 for 5 min, and incubated with the primary antibodies (mouse anti-IDH2 and rabbit anti-CytC) diluted in PBS (1:200) for 12 hr at 4°C. After three washes, all the coverslips were incubated with secondary antibodies (a mixture of FITC-conjugated antimouse IgG and Cy3-conjugated antirabbit IgG) diluted in PBS (1:250, each) for 1 hr at 23°C. After washing in PBS, Hoechst 33258 was used to stain the nucleus, and immediately, all coverslips were mounted on slides. Five HPFs were randomly selected within each coverslip, and their fluorescence was captured under LSM-700 laser confocal microscopy. Colocalization analysis was performed with the intensity correlation analysis method of the Wright Cell Imaging Facility, a plugin for Image J software. Manders overlap coefficient (MOC) as a measure of colocalization represents the proportion of normalized pixels in which two signals are colocalized (Adler and Parmryd, 2010). As MOC ranges from “0” for no colocalization to “1” for perfect colocalization, we only

considered “1” as a colocalization for clearer discrimination. The percentage (%) colocalization was determined on the basis of the ratio of the area with “1” in MOC per area with IDH2-IR (green) and averaged per group.

Western Blot Analysis

Efflux of CytC from the mitochondria to the cytosol, followed by the different treatments, was semiquantitatively measured using western blot. For this, PC-12 cells were grown in 100 Ø dish at a density of 1×10^7 cells, and the control, GLU, and GLU+NT groups were prepared as described earlier ($n=2$ wells per group). After 12 hr of incubation, the control, GLU, and GLU+NT groups were collected by centrifugation and washed twice with PBS. Cells were homogenized and subjected to cytosolic and mitochondrial fractionation by using the Mitochondria/Cytosol Fractionation Kit (Merck) in accordance with the manufacturer’s indication. Then, each of the 30-μg protein sample from both cytosolic and mitochondrial fractions was loaded to 12% sodium dodecyl sulfate-polyacrylamide gel electrophoresis, and a standard western blot analysis procedure was begun ($n=2$ per group). In brief, proteins were electrotransferred onto a polyvinylidene fluoride membrane, and then the membrane was blocked with 5% nonfat milk for 1 hr at 23°C. Next, the membranes were incubated with primary antibodies including rabbit anti-CytC, mouse anti-IDH2, and rabbit anti-GAPDH, diluted in PBS (1: 1,000 each) for 24 hr at 4°C. The IDH2 and GAPDH antibodies were used as internal controls for the mitochondrial and cytosolic fractions, respectively. After being washed three times with Tris-buffered saline containing 0.1% Tween-20, the membranes were incubated with the corresponding horseradish peroxidase-conjugated secondary antibody (1:2,000, Vector Laboratories) in a blocking solution for 2 hr at 23°C. The signals of the bound antibodies were identified with an enhanced chemiluminescence kit (Immobilon, Merck). The band intensity of CytC in cytosolic or mitochondrial fractions was measured using Image J and normalized by that of GAPDH or IDH2. Data were expressed as percentages (%) of the controls and collected from at least three independent experiments.

Statistical Analyses

All data were presented as mean ± standard error of the mean. Comparisons of the data from the different groups were performed with one-way analysis of variance (PASW Statistics version 18, SPSS Inc., Chicago, IL; RRID:SCR_002865). Differences with p values of $<.05$ were considered statistically significant. Each n value refers to the number of animals (*in vivo* experiment) or wells and coverslips (*in vitro* experiment).

Results

NT Attenuates Motor Dysfunctions in OHE Rats

To retain the reliability, prior to the NT treatment, the reproducible modeling of hepatopathic rats with maximal mimicry with the human phenotypes must be guaranteed in this study. As BDL surgery in rats is one of the most widespread experimental models to induce obstructive cholestatic liver injury (Georgiev et al., 2008; Tag et al., 2015), the major causative factor for the development of liver cirrhosis-like hepatopathy, we used this surgical technique in this study. On POD 14, gross inspection revealed that the SHAM group showed a normal liver appearance, whereas the BDL group showed a rough and yellowish surface of the liver (Figure 1(b)). In corroboration with the macroscopic findings, microscopic changes such as sinusoids widening (Figure 1(c), white arrows), bile duct distension (red asterisk), and extensive parenchymal fibrosis (white arrowheads) were also prominent in the BDL group. Furthermore, the serum levels of the liver function parameters (Table 1), including total and DBIL, AST, ALT, ALB, and NH₃ levels, were significantly altered in the BDL group, demonstrating the presence of liver dysfunction and concomitant hyperammonemia. Most importantly, parenchymal fibrosis was prominent in the livers from the BDL group as scored under the Knodell HAI. After confirmative defining of the occurrence of hepatopathy as a predisposing condition of OHE, the remained BDL groups were further divided into two groups, BDL+NT and BDL+VEH, and daily administered with either 20 mg/kg NT or normal saline as

Table 1. Serum Levels of Total, Direct Bilirubin, AST, ALT, Albumin, and Ammonia and Fibrosis Grade in the SHAM and BDL Groups at Postoperative Day 14.

	SHAM	BDL
Total bilirubin (mg/dl)	0.56 ± 0.20	6.48 ± 0.38***
Direct bilirubin (mg/dl)	0.13 ± 0.08	3.88 ± 1.76**
AST (U/L)	67.88 ± 24.70	263.66 ± 59.13***
ALT (U/L)	39.80 ± 3.70	85.40 ± 19.93**
Albumin (g/dl)	3.94 ± 0.24	3.08 ± 0.35**
Ammonia (U/L)	101.00 ± 7.17	378.80 ± 90.54***
Fibrosis grade	0.28 ± 0.48	3.22 ± 0.66***

Note. To quantify liver fibrosis, the following criteria were used in this study with the aid of the Knodell histology activity index: 0 = no fibrosis; 1 = fibrous expansion of some portal tract with or without short fibrous septa; 2 = fibrous expansion of most portal tracts with or without fibrous septa; 3 = fibrous expansion of portal tract with an occasional portal to portal bridging; 4 = fibrous expansion of portal tracts with marked portal to portal as well as portal to central bridging; and 5 = marked bridging (portal to portal and/or portal to central) with occasional nodules. Data are expressed as mean ± standard error of the mean (n = 4 per group). AST = aspartate aminotransferase; ALT = alanine aminotransferase; BDL = bile duct ligation. **p < .01 and ***p < .001 versus SHAM.

a vehicle via the i.p. route for an additional 14 days. When compared with the SHAM group, we found that the BDL+VEH group showed prominent motor deficits on the basis the significant decreases in the total distance traveled (Figure 2(a) and (b); 1,572.91 ± 618.67 vs. 2,972.10 ± 583.22 cm, **p < .01), moving speed (Figure 2(c); 3.31 ± 1.37 vs. 5.58 ± 1.02, **p < .01), and number of rearing (Figure 2(d), 23.75 ± 13.07 vs. 43.37 ± 12.86, **p < .01) under OFT. In addition, we observed a significant reduction in the ability of motor coordination in the BDL+VEH group as compared with the SHAM group, as demonstrated by the shortened latency to fall under the rotarod test (Figure 2(e); 179.66 ± 65.91 vs. 279.16 ± 26.79, ***p < .001). The result of the Y-maze task also well corroborated the results of the other behavior tests that showed a decrease in total arm entries in the BDL+VEH group as compared with the SHAM group (Figure 2(f); 15.00 ± 4.60 vs. 25.00 ± 3.63, **p < .01). However, all the reductions in motor performances, including the total distance traveled, moving speed, and number of rearing under OFT; latency to fall under the rotarod test; and total arm entries under the Y-maze test, in the BDL+VEH group, were all significantly reversed in BDL+NT group (3,090.02 ± 475.31, 5.47 ± 0.45, 50.62 ± 12.12, 257.33 ± 33.08, and 22.5 ± 1.87, respectively; #p < .05, ###p < .01, and ####p < .001 vs. BDL+VEH). No significant differences in memory performances were found in all the tested groups as revealed by the comparisons of the spontaneous alternation ratio tested under the Y-maze test (Figure 2(g); 67.34 ± 5.06, 71.39 ± 6.68, and 72.36 ± 2.89 in the SHAM, BDL+VEH, and BDL+NT groups, respectively, statistically not significant). Together, we suggest that HE-associated motor deficits can be attenuated by the treatment with NT even if the initial treatment started from when the hepatopathy is already obvious, that is, in the OHE stage.

NT Attenuates Neuronal Death Without Affecting Astroglia in SNc in OHE Rats

Among various subsets of CNS known to be affected by HE, SNc and DA-ergic neurons have been revealed to be specifically susceptible to HE (Maddison, 1992; Yamada et al., 1992; Jones and Weissenborn, 1997; Dhanda and Sandhir, 2015). On the basis of this view, we evaluated the potential therapeutic effect of NT against OHE by observing histological changes in the SNc. As expected, we revealed that neurotoxic findings were evident in the SNc of BDL+VEH, demonstrating a significant reduction in the number of cresyl-violet-stained SNc DA-ergic neurons as compared with that in SHAM (Figure 3(a) and (b), 7.80 ± 2.58 vs. 17.71 ± 3.45, ***p < .001). However, the GLU+NT group exhibited a significant increase in the number of SNc DA-ergic neurons

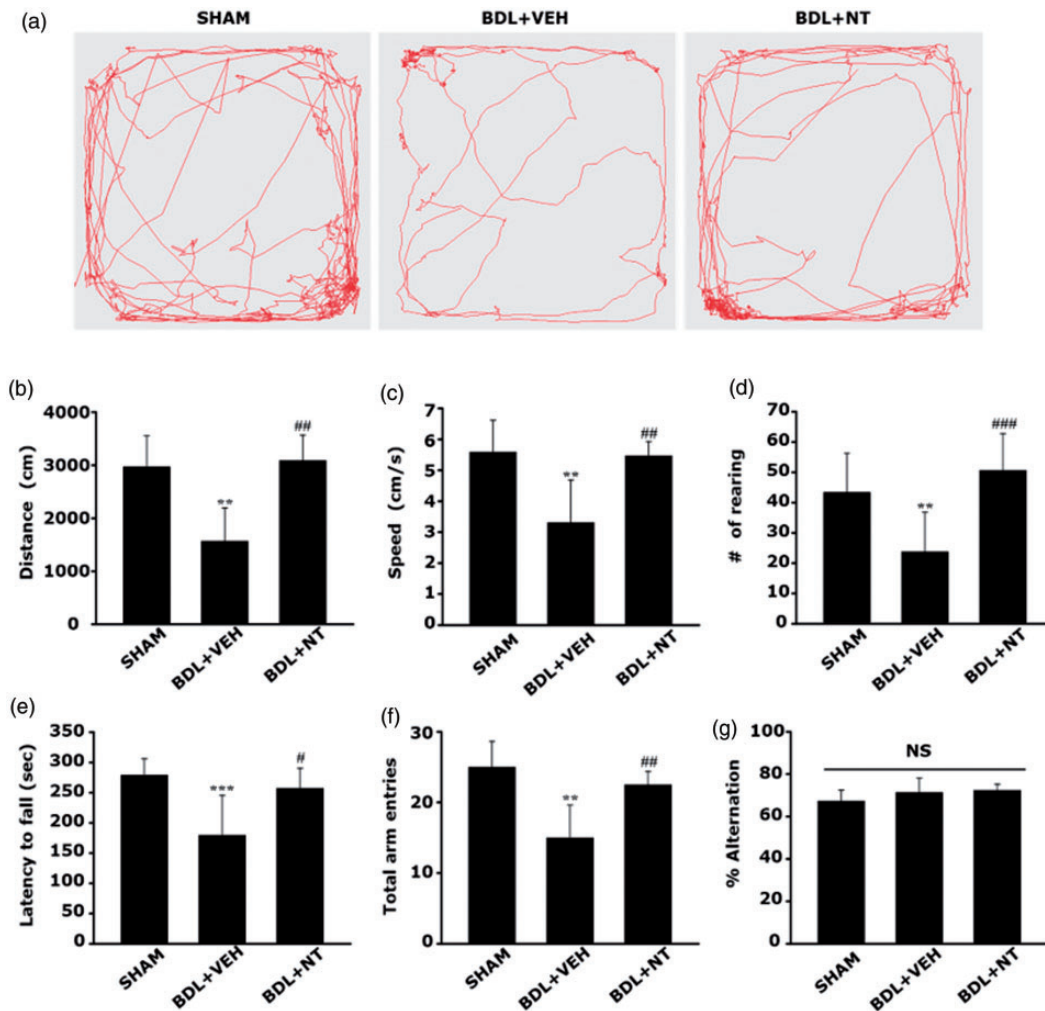


Figure 2. Attenuation of motor dysfunction in OHE rat by NT administration. The behavioral assessment of motor and memory functions in the SHAM, BDL+VEH, and BDL+NT groups. (a to d) Open-field test executed at POD 25. (a) Representative tracks of SHAM, BDL+VEH, and BDL+NT groups in the open-field chamber over 10 min. (b) The averaged total distance traveled, (c) speed, and (d) number of rearing over 10 min. (e) The averaged latency to fall under the rotarod test executed at POD 26. The velocity of the rod rotation was accelerated from 4 to 40 rpm over a 5-min period. (f and g) The Y-maze test executed at POD 27. (f) The average total number of arm entries over 8 min and (g) alternation rate calculated with the following formula: alternation rate (%) = number of alternations/(number of total arm entries - 2) × 100. All bar graphs represent mean ± standard error of the mean ($n = 12$ per group). ** $p < .01$ and *** $p < .001$ versus SHAM; # $p < .05$, ## $p < .01$, ### $p < .001$ versus BDL+VEH. NS = statistically not significant; BDL = bile duct ligation; VEH = vehicle; NT = nortriptyline.

compared with the GLU group (16.6 ± 3.91 , ## $p < .01$). Considering that TH, a rate-limiting dopamine-synthesizing enzyme, is used as a specific indicator of synaptic integrity in the nigrostriatal pathway, we revealed that BDL+VEH exhibited a dramatic loss in synaptic densities by demonstrating that TH-IRs significantly decreased in the neurophil regions of the SNc (Figure 3(c) and (d)) and striatum (Figure 3(e) and (f)), which are reminiscent of the presynaptic and postsynaptic sprouts that composed the nigrostriatal pathway, respectively. However, the BDL+NT group exhibited significant increases in the values as compared with the

BDL+VEH group ($88.68\% \pm 14.85\%$ vs. $50.06\% \pm 13.54\%$ and $98.55\% \pm 12.13\%$ vs. $71.62\% \pm 10.31\%$, # $p < .05$). It is interesting that as immunohistochemical detection of GFAP revealed that astrogliosis in the SNc seemed to be prominent in the BDL+VEH group when compared with the SHAM group (491.83 ± 80.62 vs. 100 ± 16.77 , ** $p < .01$), no significant differences were found in those extents between the BDL+VEH and BDL+NT groups (Figure 3(g) and (h); 491.83 ± 80.62 vs. 440.98 ± 80.03 , statistically not significant). Thus, we could rule out the involvement in the secondary effect, that is, the possible modulation of astrocytes, from the

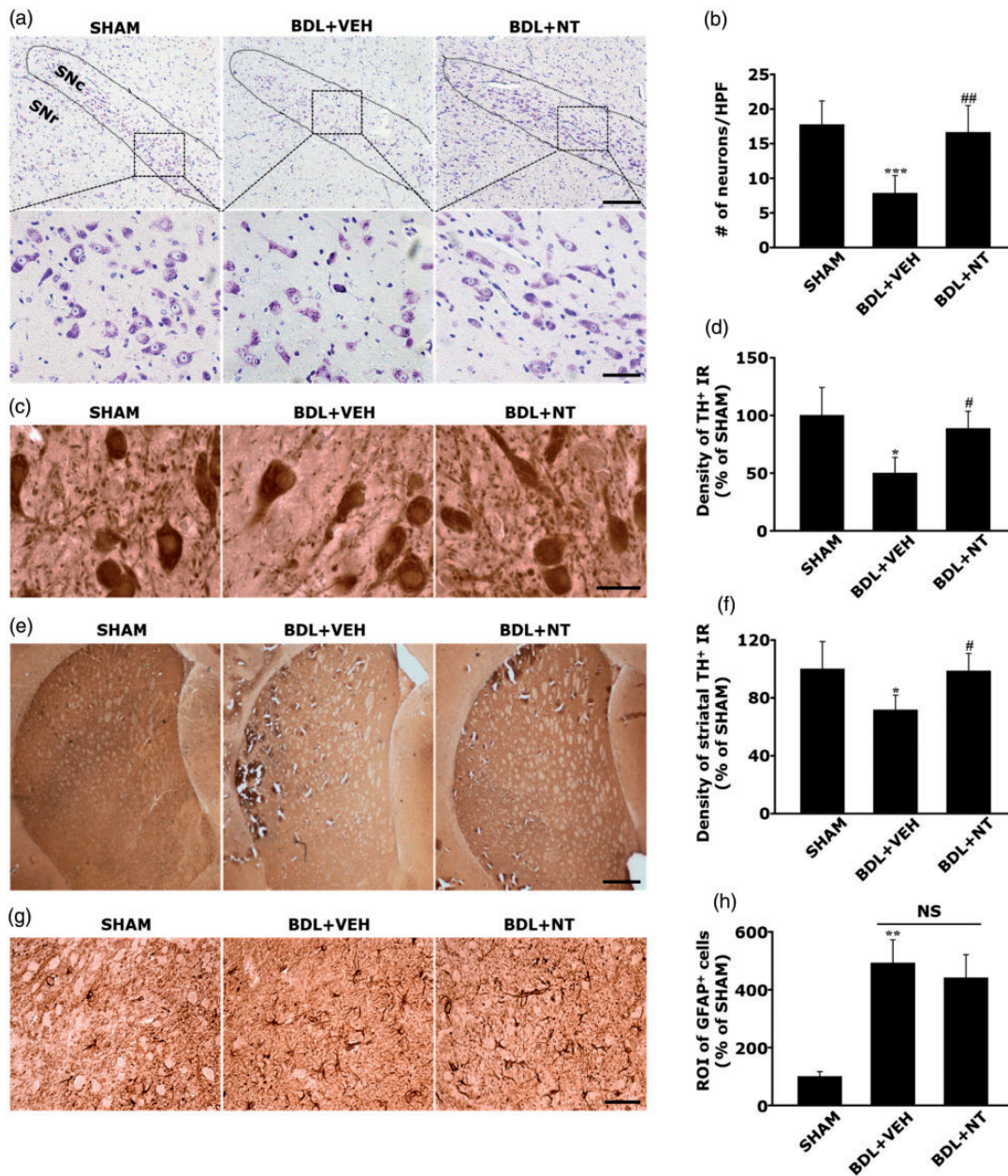


Figure 3. Attenuation of neuronal death without affecting astrogliosis in SNc in OHE rats by NT administration. (a) Representative cresyl-violet-stained images of SNc in SHAM, BDL+VEH, and BDL+NT groups. SNc is depicted with the area bounded with a dotted line. For a clearer visualization, the rectangular boxed areas in upper panels (100 \times) are magnified as shown in lower panels (400 \times). Scale bar = 200 and 50 μ m in upper and lower panels, respectively. (b) The average number of SNc neurons. Neuronal cell bodies with visible nucleoli were only counted. Representative TH immunohistochemistry images of SNc (c) and striatum (e) and the averaged TH immunoreactivities in SNc (d) and in striatum (f). Scale bar = 20 and 500 μ m in panels (c) and (e), respectively. (g) Representative GFAP immunohistochemistry images and (h) the averaged GFAP immunoreactivities in SNc. Scale bar = 50 μ m. To quantify the immunoreactivities of TH and GFAP, the randomly selected brain sections contained with SNc or striatum were photographed under the different magnification values. The ROI per high-power field were analyzed by Image J (v.1.49) and averaged per group. For all graphs, data are expressed as percentage of SHAM group ($n = 8$ per group). * $p < .01$, ** $p < .01$, *** $p < .001$ versus SHAM group; # $p < .05$, ## $p < .01$ versus BDL+VEH group. BDL = bile duct ligation; VEH = vehicle; NT = nortriptyline; SNr = substantia nigra reticulata; NS = statistically not significant; GFAP = glial fibrillary acidic protein; TH = tyrosine hydroxylase; ROI = relative optical intensity; IR = immunoreactivity.

therapeutic mechanism of NT. We suggest that the HE-associated histological deterioration of the DA-ergic neurons in the nigrostriatal pathway can be protected by the neuron-specific protective effects of the NT.

NT Inhibits Neuronal Apoptosis and Mitochondrial Damage in the SNc in OHE Rats

To address the involvement in apoptosis cascade and mitochondrial pathology in the context of the neuroprotective action of NT on OHE, we quantitatively assessed the apoptosis extent and qualitatively monitored the mitochondrial ultrastructures in SNc neurons by using the TUNEL assay and TEM, respectively. If the TUNEL-positive apoptotic neurons were hardly detectable in the SNc of the SHAM group, these were markedly increased in the BDL+VEH group (Figure 4(a) and (b), 1.80 ± 1.30 vs. 29.00 ± 8.36 , $***p < .001$). However, the amount of TUNEL-positive apoptotic neurons in the SNc were significantly diminished in the BDL+NT group (19.2 ± 4.96 , $\#p < .05$). In addition, TEM observation revealed that of the SHAM group, the mitochondria possess well-defined cristae within the matrix. However, the BDL+VEH group showed an aberrant mitochondrial morphology such as swelling, disruption of the cristae, and even cristalysis (Figure 4(c), indicated as an arrowhead) in the SNc neurons. Notably, when compared with the BDL+VEH group, most aberrant mitochondrial

morphologies in the SNc neurons were remarkably attenuated in the BDL+NT group, although the uneven distention of the intercrisetae space was still presented (indicated as an asterisk). Together, we can suggest that NT confers the neuroprotection on OHE-associated SNc DA-ergic neurotoxicity through the inhibition of apoptosis and concomitant protection of mitochondrial ultrastructures.

NT Attenuates the DA-ergic Cell Death Caused by Glutamate Excitotoxicity

Considering the key role of GE on OHE-associated neurotoxicity as described earlier, we used the neuron-like cell line challenged with GE as an *in vitro* model of OHE. To give a maximal mimicry with the SNc DA-ergic neuron *in vivo*, a rat pheochromocytoma PC-12 cell, which is widely accepted as a DA-ergic line due to the releasing property of DA and the expression of DA receptors, was used in this study as an *in vitro* model system. First, PC-12 cells were treated with various concentrations of glutamate (0–20 mM) and NT (0–100 μ M) for 24 hr to estimate the LD₅₀ and the MAC of NT, respectively. After obtaining the LD₅₀ values of glutamate and MAC of NT as 15 mM (Figure 5(a)) and 10 μ M (Figure 5(b)), respectively, the 24-hr viabilities of the control, GLU, and GLU+NT groups that were prepared with the protocol described earlier (“Materials and

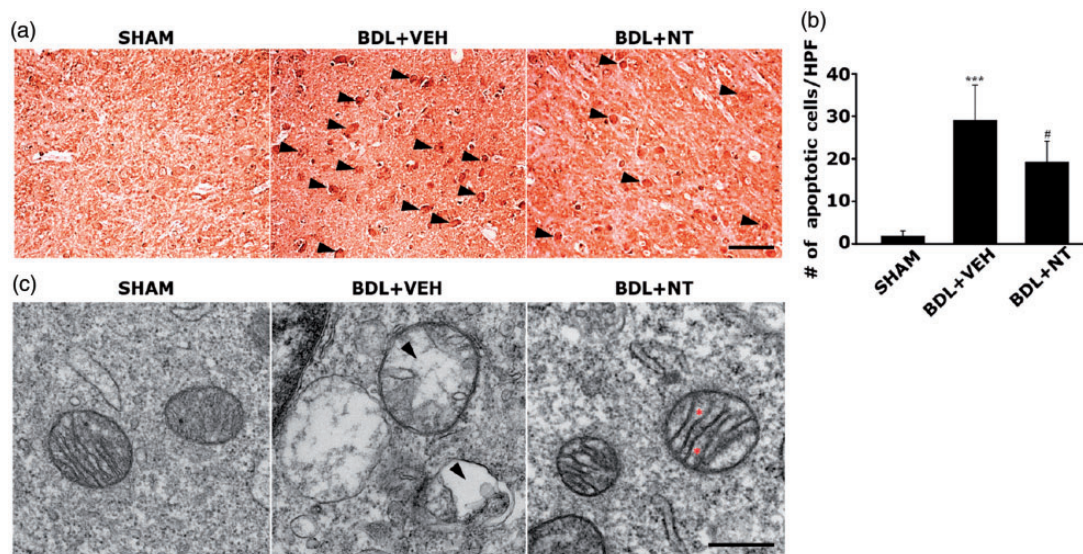


Figure 4. Inhibition of neuronal apoptosis and mitochondrial damage in SNc of OHE rat by NT administration. (a) Representative TUNEL-assayed images of SNc in the SHAM, BDL+VEH, and BDL+NT groups. TUNEL reactivities were first classified into three categories: TUNEL⁺ (low), TUNEL⁺⁺ (moderate), and TUNEL⁺⁺⁺ (high) and next, the TUNEL⁺⁺⁺ neurons, as indicated with arrowheads in (a), were only counted as TUNEL-positive. Scale bar = 50 μ m. (b) The average numbers of TUNEL-positive neurons. All bar graphs represent mean \pm standard error of the mean ($n = 8$ per group). $***p < .001$ versus SHAM group; $\#p < .05$ versus BDL+VEH group. (c) Representative TEM images showing mitochondrial morphology in SNc neurons of different groups ($n = 4$ per group). Scale bar = 500 nm. The cristalysis and distention of the intercrisetae space are depicted with arrowheads and asterisks. BDL = bile duct ligation; VEH = vehicle; NT = nortriptyline.

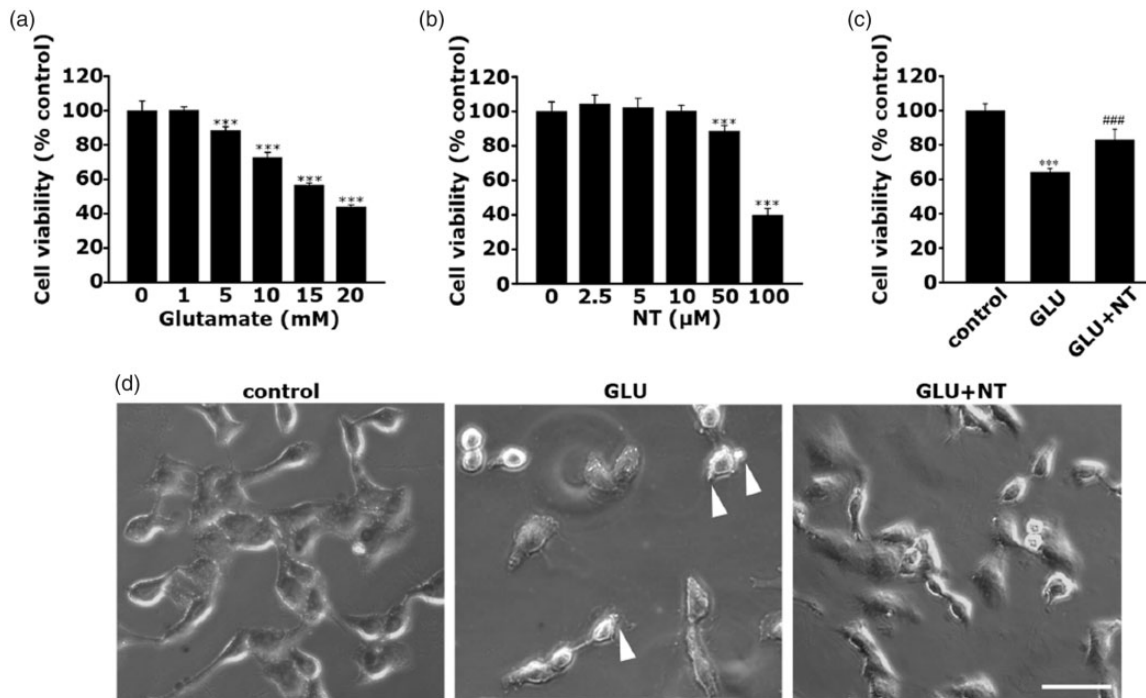


Figure 5. Protective effect of NT on glutamate excitotoxicity-induced death of PC-12 cells. (a) Dose-dependent cell viability of PC-12 cells following incubation with varying concentrations of glutamate (0, 1, 5, 10, 15, and 20 mM) for 24 hr. $***p < .001$ versus cells untreated with glutamate. (b) Dose-dependent cell viability of PC-12 cell following incubation with varying concentrations of NT (0, 2.5, 5, 50, and 100 μ M) for 24 hr. $***p < .001$ versus cells untreated with NT. As revealed in (a) and (b), it was determined that the median lethal dose (LD_{50}) of glutamate and maximum allowable concentration of NT are 15 mM and 10 μ M, respectively; thus, those concentrations were selected as the optimal doses for evoking glutamate excitotoxicity and applied for all the subsequent *in vitro* studies. In this regard, each PC-12 cell group treated with vehicle, 15 mM glutamate, or 15 mM glutamate plus 10 μ M NT will be referred to as control, GLU, or GLU+NT groups, respectively. (c) Cell viability of control, GLU, and GLU+NT groups tested at 24 hr after the different treatments. All bar graphs represent mean \pm standard deviation in at least three independent experiments ($n = 8$ wells per group). $***p < .001$ versus control; $####p < .001$ versus GLU group. (d) Representative cell images captured using an inverted microscope for the different groups. Membrane blebblings are depicted with a white arrowhead. Scale bar = 25 μ m. GLU = glutamate; NT = nortriptyline.

Methods" section) were analyzed. The GLU group showed reduced viability than the control group (Figure 5(c); $64.10\% \pm 2.15\%$ vs. $100\% \pm 3.98\%$, $***p < .001$); however, the GLU+NT group showed increased viability ($82.83\% \pm 6.40\%$, $####p < .001$). The neuroprotective effect of NT was also confirmed by morphological observation using a phase-contrast microscope (Figure 5(d)). The GLU group showed the typical hallmarks of cell death, including diminution of cellular processes, membrane blebbing (indicated by the white arrowhead), and cell shrinkage. These morphological features markedly recovered in the GLU+NT group. These results indicated that NT treatment confers protection on DA-ergic cells against GE.

NT Attenuates Apoptosis of DA-ergic Cell Apoptosis Caused by Glutamate Excitotoxicity

To confirm that GE-induced PC-12 cell death is due to the apoptotic death and to assess the inhibitory role of

NT on this, we performed morphology- and flow cytometry-based apoptosis assays. At 12 hr after the different treatments, nuclear stain with Hoechst 33258 revealed that the GLU group showed the typical morphology of apoptotic shrunken nuclei with irregular contour (Figure 6(a); white arrowhead) and a marked increase in the number of shrunken nuclei as compared with the control, which had uniform round-shaped nuclei (Figure 6(b), $44.65\% \pm 10.14\%$ vs. $4.01\% \pm 3.75\%$, $***p < .001$). However, the GLU+NT group displayed a significant reduction in the number of shrunken nuclei as compared with those of the GLU group ($18.99\% \pm 4.56\%$, $####p < .001$). We further confirmed our results with the aids of flow cytometry with Annexin V-FITC/PI staining. The percentage of the total cell population ongoing apoptosis was abruptly increased in the GLU group as compared with the control group (Figure 6(c) and (d); $43.47\% \pm 1.53\%$ vs. $3.78\% \pm 0.94\%$, $***p < .001$); however, the GLU+NT group showed a significant reduction in value to a

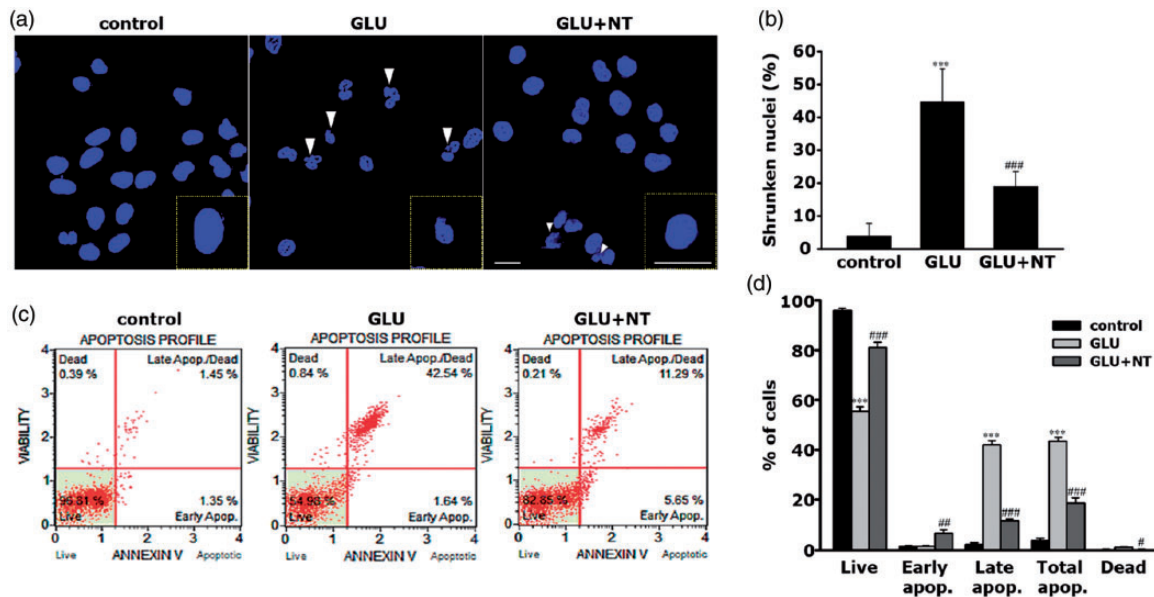


Figure 6. Protective effect of NT on glutamate excitotoxicity-induced apoptosis of PC-12 cells. (a) Representative Hoechst 33258-stained images of the control, GLU, and GLU+NT cell groups obtained at 12 hr after the different treatment. The white arrowhead indicates shrunken nuclei with irregular contour, the typical appearance of apoptotic nuclei. A magnified view of nuclei with the typical morphology is supplied in inlets. Scale bar = 10 μ m. (b) The average ratio of shrunken nuclei in total nuclei per a HPF ($n = 4$ coverslips per group). (c) Representative dot plot diagrams obtained by flow cytometry analysis of different cell groups after staining with Annexin V-FITC/PI. The plots are divided into four quadrants so that live cells fall into the lower left quadrant (Annexin V-negative, PI-negative), early apoptosis is at the lower right quadrant (Annexin V-positive, PI-negative), late apoptosis is at the upper right quadrant (Annexin V-positive, PI-positive), and the dead cells are at the upper left quadrant (Annexin V-negative, PI-positive). (d) Live, apoptotic (early, late, and total), and dead cells were quantified by Muse[®] Cell Analyzer after Annexin V-FITC/PI labeling. Bar graphs represent mean \pm standard error of the mean ($n = 4$ wells per group) in at least three independent experiments. $***p < .001$ versus control; $###p < .01$, $####p < .001$ versus GLU group. GLU = glutamate; NT = nortriptyline.

percentage of $18.68\% \pm 2.08\%$ ($####p < .001$). These results suggest that NT treatment can attenuate GE-induced DA-ergic neurotoxicity mainly through inhibition of apoptosis.

NT Attenuates Glutamate Excitotoxicity-Induced Mitochondrial Dysfunction in DA-ergic Cells

In line with the accumulating evidence that impaired mitochondrial biogenesis is closely associated with HE (Rao and Norenberg, 2012; Dhanda et al., 2018), we assessed the functional integrity of neuronal mitochondria by using a mitochondrial respirometer. The results demonstrated that the 12-hr OCRs under the different respiratory conditions were globally decreased in the GLU group as compared with the control group. In detail, as shown in Figure 7(a), an illustration of a representative experiment depicting changes in OCR under different respiratory conditions defined by the sequential injections of oligomycin, FCCP, and a mixture of rotenone and antimycin A, glutamate hampered the mitochondrial respiratory parameters, which were significantly reversed by NT cotreatment.

Specifically, a marked reduction in basal respiration was observed in the GLU group as compared with the control group (Figure 7(b), 17.24 ± 8.17 vs. 37.07 ± 1.19 , $**p < .01$), and the GLU+NT group failed to reverse the reduction (21.05 ± 5.50 , statistically not significant). However, while the GLU group showed a potent reduction in ATP-linked respiration to a subzero level (Figure 7(c); -4.42 ± 1.29 vs. 28.53 ± 0.70 , $***p < .001$ vs. control) with corresponding increases in the proton leak (Figure 7(d); 21.66 ± 6.87 vs. 8.54 ± 0.48 , $***p < .001$ vs. the control), the value was significantly normalized in the GLU+NT group (14.62 ± 4.65 , $####p < .001$ and 6.42 ± 0.84 , $####p < .001$, respectively). Furthermore, the GLU group displayed a decrease in mitochondrial respiration to a level even below 0 (Figure 7(e); -2.19 ± 4.47 vs. 58.96 ± 7.86 , $***p < .001$ vs. the control) with the presence of the chemical uncoupler FCCP, an indicator of maximal respiration. However, the GLU+NT group showed a significant reversal in this reduction (25.34 ± 9.04 , $####p < .001$). These results suggest that NT can preserve the mitochondrial function in DA-ergic cells against the GE.

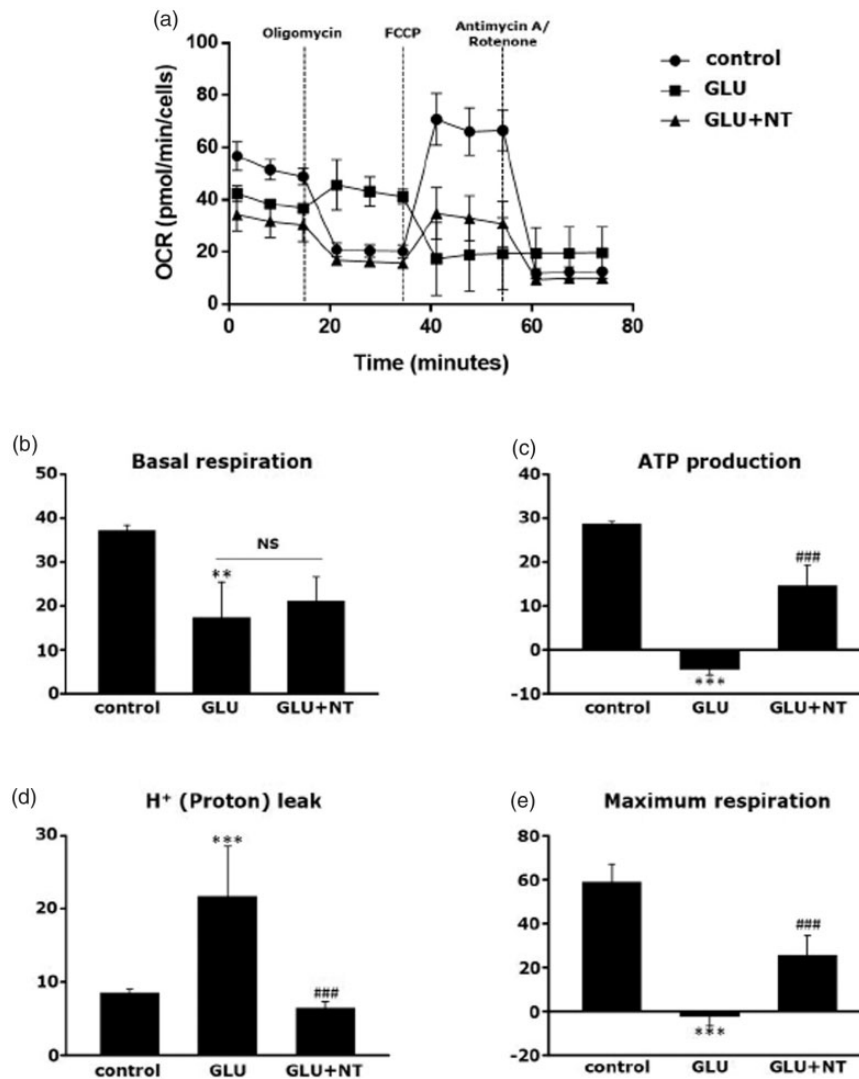


Figure 7. Attenuation of glutamate excitotoxicity-induced mitochondrial dysfunction in PC-12 cells by NT treatment. (a) The OCRs of control, GLU, and GLU+NT groups assessed by Seahorse XF24 extracellular flux analyzer at 12 hr after different treatments. OCR was measured under basal conditions, followed by the sequential additions of oligomycin (10 μ M), FCCP (3 μ M), and rotenone (10 μ M) + antimycin A (10 μ M) at each time points as indicated in OCR curve. Each data point represents an OCR measurement. Individual parameters for (b) basal respiration, (c) ATP production, (d) proton leak, and (e) maximum respiration. Cells of different groups were seeded at a density of 5×10^4 cells/well in XF24 cell culture microplates and each OCR was normalized by the number of viable cells. Bar graphs represent mean \pm standard error of the mean ($n = 4$ wells per group) in at least three independent experiments. ** $p < .01$ and *** $p < .001$ versus control; ### $p < .001$ versus GLU group. GLU = glutamate; NT = nortriptyline; OCR = oxygen consumption rate; ATP = adenosine triphosphate; FCCP = carbonyl cyanide-4-(trifluoromethoxy)phenylhydrazone.

NT Inhibits Glutamate Excitotoxicity-Induced CytC Translocation and $\Delta\Psi_m$ Perturbation in DA-ergic Cells

Our major thrust in this study was to screen the therapeutic effect in OHE after treatment with NT, the agent newly discovered to block the mPTP. Together with the notion of the well-known property of mPTP as a pore of CytC efflux from the mitochondrial matrix to the cytosol, we morphologically and semiquantitatively studied the inhibitory action of NT on CytC translocation.

As shown in Figure 8(a), immunofluorescence observation under confocal microscopy and the highlighted images revealed that most CytC (red) remained in the IDH2-IR mitochondria (green) in the control group as depicted by the widespread yellow dots in the merged image. As expected, while the GLU group showed a significant decrease in the yellow dots in the merged image, suggesting the mobilization of a large amount of CytC from the mitochondria to the cytosol, the GLU+NT group displayed a marked reversal in this fluorescent

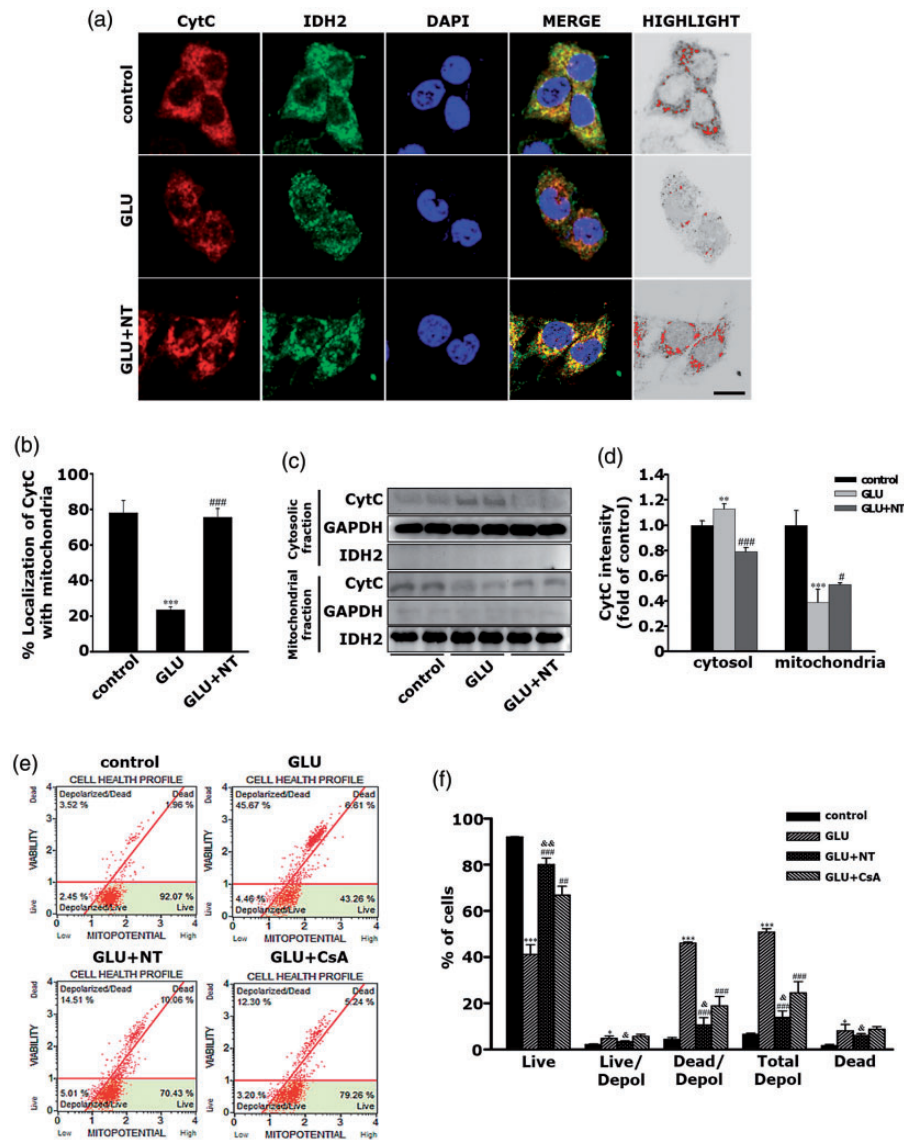


Figure 8. Attenuation of glutamate excitotoxicity-induced CytC translocation and $\Delta\Psi_m$ perturbation in PC-12 cells by NT treatment. (a) Representative images showing CytC colocalization with mitochondria in PC-12 cells of the control, GLU, and GLU+NT groups obtained at 12 hr after the different treatments. Cells were probed with antibodies against CytC (red) and IDH2 (green), a mitochondrial marker. Hoechst 33258 (blue) used as a nuclear marker. Yellow dots in the merged figures indicate that CytC remained in mitochondria. The area with “I” in the MOC value obtained under the colocalization analysis was highlighted by pseudocoloration with red overlaying a gray-scaled background. Scale bar = 10 μ m. (b) Quantification of percentage (%) colocalization by using Image J/Wright Cell Imaging Facility plugin ($n = 4$ coverslips per group). (c) Representative immunoblots to estimate the amount of CytC expression in mitochondrial and cytosolic protein fractions. GAPDH and IDH2 were used as housekeeping controls for cytosolic and mitochondrial proteins, respectively. (d) The average band intensities of CytC in mitochondrial and cytosolic protein fractions. Band densities of CytC in cytosolic or mitochondrial fractions were normalized by those of GAPDH or IDH2, respectively, and converted by folds of the controls. Bar graphs represent mean \pm standard error of the mean (SEM) in at least three independent experiments ($n = 2$ per group). (e) Representative dot plot diagrams obtained by flow cytometry analysis of different cell groups after Muse[®] Mitopotential assay. The CsA was used as a positive control. The plots are divided into four quadrants, so that live cells fall into the upper right quadrant, live cells with depolarized $\Delta\Psi_m$ at the lower left quadrant, dead cells with depolarized $\Delta\Psi_m$ at the upper left quadrant, and dead cells at the lower right quadrant. (f) Live cells, live or dead cells with depolarized $\Delta\Psi_m$, and dead cells were quantified by Muse[®] Cell Analyzer. Bar graphs represent mean \pm SEM in at least three independent experiments ($n = 4$ wells per group). * $p < .05$, ** $p < .01$, *** $p < .001$ versus control; # $p < .05$, ### $p < .01$, #### $p < .001$ versus GLU; & $p < .05$, && $p < .01$ versus GLU+CsA. GLU = glutamate; NT = nortriptyline; CsA = cyclosporine A; CytC = cytochrome C; GAPDH = glyceraldehyde-3-phosphate dehydrogenase; IDH = isocitrate dehydrogenase.

changes. The comparisons of percentage colocalization further clarified that the GLU group showed a dramatic reduction in the mitochondrial CytC (Figure 8(b); 23.42 ± 2.09 vs. 78.33 ± 5.36 , $***p < .001$ vs. the control), which significantly normalized in the GLU+NT group (77.68 ± 3.97 , $###p < .001$). Furthermore, as shown in Figure 8(c) and (d), the semiquantitative western blot experiments revealed the corroborated data that the GLU group showed a marked reduction in CytC level in mitochondrial fraction (0.38 ± 0.10 vs. 1.00 ± 0.11 , $***p < .001$) and an inverse elevation in cytosolic fraction (1.13 ± 0.04 vs. 1.00 ± 0.03 , $**p < .01$) when compared with the controls. However, GLU+NT displayed significant reversals on these changes (0.52 ± 0.01 , $#p < .05$ and 0.79 ± 0.03 , $###p < .001$, respectively). As the disruption of $\Delta\Psi_m$ and the resulting depolarization are strongly believed to coincide with the opening of the mPTP (Ruiz-Meana et al., 2007; Gyulhandanyan et al., 2015), we assayed the $\Delta\Psi_m$ after the different treatments to quantify the extent of the mPTP opening. The result showed that the GLU group had a marked increase in percentage of cells with depolarized $\Delta\Psi_m$ (Figure 8(e) and (f); 50.80 ± 1.49 vs. 6.49 ± 0.51 , $***p < .001$ vs. the control), whereas the GLU+NT group showed a significant attenuation in this value (13.89 ± 2.75 , $###p < .001$ vs. GLU). The inhibitory action of NT on $\Delta\Psi_m$ depolarization seemed to be even higher than that of cyclosporin A (24.49 ± 4.85 , $^{\&}p < .05$), a classical mPTP blocker used as a positive control. Together, these results suggest that the pharmacological mechanism underlying the protection of NT on DA-ergic cells against GE involves, at least in part, the attenuation of mitochondrial dysfunction by inhibiting CytC translocation and $\Delta\Psi_m$ perturbation.

Discussion

To our knowledge, this study, besides reporting the well-known involvement in GE-induced DA-ergic neurotoxicity on the progression of OHE, documents for the first time the following: (a) the neuroprotective effects of NT administration in a rat model of OHE and (b) the participation of the structural and functional protection of mitochondria in the therapeutic mechanism of NT on GE-induced DA-ergic neurotoxicity associated with OHE. Although further studies are needed to clarify the additive therapeutic mechanism of NT on this disease, we demonstrated the obvious therapeutic efficacy of NT on neurobehavioral symptoms and histological deteriorations that are commonly accompanied with OHE and the involvement in mitochondrial dysfunction attenuation as, at least in part, one of the key mechanisms underlying the therapeutic efficacy of NT on OHE.

As stated earlier, numerous studies have shown that hyperammonemia acts as a key causative factor for the

pathogenesis of OHE (Rodrigo et al., 2010; Ciećko-Michalska et al., 2012; Felipo et al., 2012). Thus, the modalities to reduce the NH_3 burden by nonabsorbable disaccharides such as lactulose are currently suggested as the gold standard treatment for OHE (Montagnese et al., 2004; Liu et al., 2017). Unfortunately, some limitations remain to be overcome in the therapeutic use of nonabsorbable disaccharides as an OHE therapeutic. First, long-term and randomized clinical trial-based scientific studies regarding the side effects of these medication, possibly outweighing the benefits, are relatively lacking (Hannan, 2008; Every-Palmer and Howick, 2014). Although lactulose was introduced as a safer alternative for antibiotics as a therapeutic option for OHE, patients with this medication in clinical settings commonly experience severe diarrhea, nausea, and abdominal discomfort (Al Sibae and McGuire, 2009). In fact, comorbid occurrence of dehydration or electrolyte imbalance has the potential to worsen the outcomes, actually triggering the recurrence of HE (Mina Shaker and Carey, 2014). More important is the second point, which is that the successful salvation of hyperammonemia with this medication does not always guarantee the corresponding therapeutic response because serum NH_3 level does not precisely correlate with the severity of the neuropsychiatric symptoms associated with OHE (Basile and Mullen, 2009; Swaminathan et al., 2018). We assumed that the possible cause of this discrepancy can be explained with an indirect, astrocyte-mediated action of NH_3 on neurotoxicity. Thus, when the indirect toxin rapidly disappears, elevation of the extraneuronal glutamate level still might trigger the GE-induced neurotoxicity for a longer duration. Thus, screening of novel therapeutic modalities that can directly act on neurons challenged with GE, not on astrocytes coping with hyperammonemic insult, was the primary aim of this study.

To accomplish this aim, we used BDL rats as an *in vivo* experimental model of OHE according to the members of the International Society for Hepatic Encephalopathy and Nitrogen Metabolism commission on experimental models of HE. BDL rats were described to develop multiorgan symptoms associated with OHE, including hepatic failure, jaundice, portal hypertension, bacterial translocation in the gastrointestinal tract, immune system dysfunction, hyperammonemia, and encephalopathy (Butterworth et al., 2009). By using this animal model, we collected evidence of the occurrence of motor disturbances. These findings were of great interest because the nigrostriatal pathway that plays a crucial role in motor control has been recognized as the one of most susceptible subsets in relation to HE pathologies. On this basis, the present study used three batteries of behavioral tests, including the open-field, rotarod, and Y-maze test, and demonstrated that BDL+VEH rats exhibited decreases in locomotor activity and motor coordination,

both of which were significantly reversed in the BDL+NT rats. The motor deficits of the BDL+VEH rats shown in this study well corroborate the previous results of other studies (Chen et al., 2014; Giménez-Garzó et al., 2015). However, a discrepancy was found in the memory performance result shown in the BDL+VEH rats. That is, while both clinical and experimental HE models are known to be commonly accompanied with the discrete loss of memory function, it showed no difference in memory function between the BDL+VEH and SHAM groups as demonstrated in the Y-maze test. We suggest that this discrepancy is due to the differences in susceptibility to BDL between the hippocampus, a region responsible for memory function, and the other motor-responsible regions such as SNc, although further memory function tests might be additionally needed to address this issue.

In this study, we selected the nigrostriatal DA-ergic neurons as the cellular target of protection possibly conferred by the NT. As the first study reported the

reduction in TH-IR SNc neurons after porto-caval anastomosis onto rats, an alternative model of HE, in 1991, to date, a few studies have described the neurotoxic effects of HE on the nigrostriatal DA-ergic neurons *in vivo* (Cauli et al., 2009; El Hiba et al., 2016). Among these, a recent study that aimed to reveal the therapeutic action of combinatorial delivery of genes, namely, human plasminogen activator and matrix metalloproteinase-8, used nigrostriatal DA-ergic neurons as the regional target for gene delivery (Gálvez-Gastélum et al., 2010). A few studies *in vitro* also have shown that DA-ergic neurons are preferentially affected by glutamate toxicity (Kikuchi and Kim, 1993; Casper et al., 2000). One of these studies reported that DA-ergic neurons exposed to glutamate for 24 hr were more vulnerable than non-DA-ergic neurons exposed to glutamate for more than 24 hr (Izumi et al., 2009). These reports might suggest that the specific susceptibility of DA-ergic SNc neurons to GE is profoundly involved in HE progression. Together with these reports, the results of present study might call

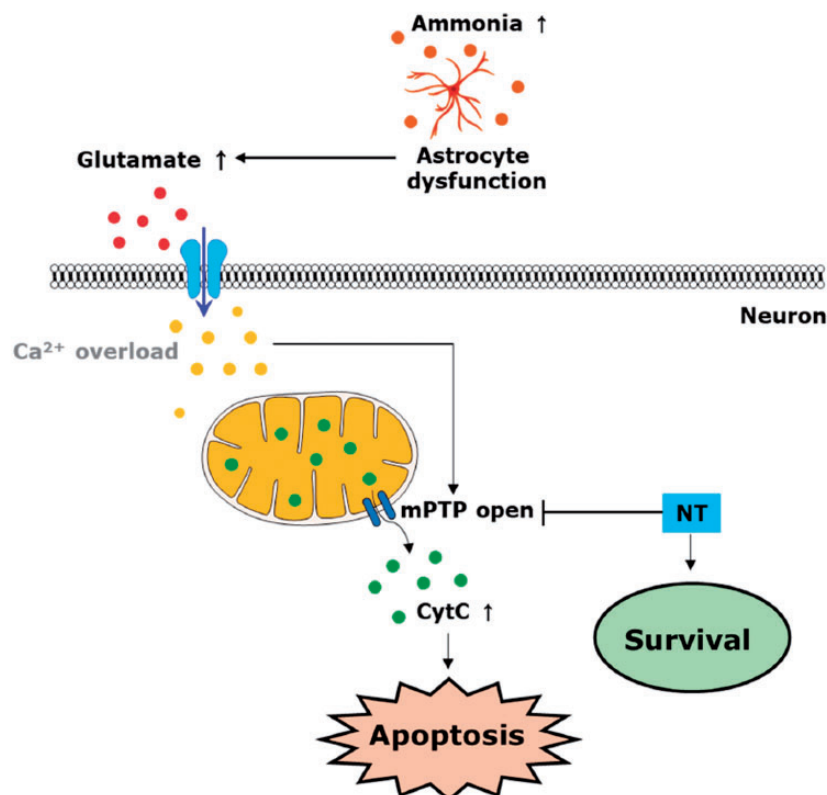


Figure 9. Summary. A schematic diagram showing the neuroprotective roles of NT in an OHE model. Hyperammonia triggered by OHE renders the astrocyte to be dysfunctional; thus, glutamate becomes accumulated in the extraneuronal space. Once the so-called glutamate excitotoxicity initiates, the increased glutamate–glutamate receptor interactions cause cytosolic calcium overload, and subsequently results in an opening of the mPTP via presumably complex and multifactorial mechanisms. The opened mPTP renders the CytC to translocate from the mitochondria to cytosol, thus resulting in the apoptotic death of neurons, including SNc DA-ergic neurons. The administration of NT can rescue the neurons against the OHE-associated neurotoxicity by inhibiting mPTP-mediated neurotoxic mechanisms, for example, CytC translocation and mitochondrial dysfunction. mPTP = mitochondrial permeability transition pore; NT = nortriptyline; CytC = cytochrome C.

attention to the nigrostriatal DA-ergic neurotransmission as an important therapeutic target region for OHE therapeutics.

The selection of NT as the candidate drug of this study was initially inspired by the excellent research paper published in 2004, which was the first to demonstrate the lowering effect of NT on mPT in the isolated mitochondria from rat hepatocytes (Stavrovskaya et al., 2004). In that paper, quantification of the modulatory property of NT on mPT was based on the measurement of mitochondrial swelling, mitochondrial respiration, and $\Delta\Psi_m$ values. Thus, as the authors also described, their study had some limitations as follows: (a) the use of isolated mitochondria, but not the target tissue and (b) the possible existence of unrecognized target of NT other than mPTP. Here, we could partially overcome the former problem by employment of PC-12 cells, the cell line widely used as an *in vitro* DA-ergic neuronal cell line. However, the latter problem, which is the unrecognized *off-target* effect of NT, for example, its possible interactions with the norepinephrine transporters (Takano et al., 2014) and α 1-adrenergic receptor (Nojimoto et al., 2010), remains to be further investigated. For this, multidisciplinary approaches consisting of well-defined biochemical analyses and even computational methods such as molecular docking study can provide deeper insight into the action machinery of NT.

Another remaining caveat in this study is the non-observance of the possible effect of NT on concomitant hepatic protection. Considering that the mitochondria are a universal organelle, NT can exert a concomitant hepatoprotective effect of course; in turn, this confounding effect might have substantially influenced the neuroprotective effects of the NT that we observed in this study. Thus, further experiment to rule out the contribution of the possible hepatic protection by 2 weeks of NT treatment is needed. Furthermore, as we did not include an experimental group that was sham-operated and subsequently administrated with NT, we cannot exclude the possibilities that NT could affect the basal status of locomotor activities, DA-ergic neuronal number, or mitochondrial turnover, which would suggest a *health-promoting* effect of NT treatment.

In conclusion, combining the *in vivo* and *in vitro* results, this study suggests that NT can exert a therapeutic role against OHE, mitigating the GE-induced neurotoxicity via inhibition of mPTP-associated mitochondrial dysfunction in SNc DA-ergic neurons (Figure 9). Therapeutic targeting of mitochondrial dysfunction with mPTP blockers, including NT, might open a new era for future research studies aimed at OHE therapeutics development.

Declaration of Conflicting Interests

The author(s) declared no potential conflicts of interest with respect to the research, authorship, and/or publication of this article.

Funding

The author(s) disclosed receipt of the following financial support for the research, authorship, and/or publication of this article: This work was supported by funds from Korea Research Foundation (grant no. NRF-2016R1C1B2012351, NRF-2017R1C1B2006365, and NRF-2017R1D1A3B04034812).

References

- Adler, J., & Parmryd, I. (2010). Quantifying colocalization by correlation: The Pearson correlation coefficient is superior to the Mander's overlap coefficient. *Cytometry A*, 77A, 733–742.
- Al Sibae, M. R., & McGuire, B. M. (2009). Current trends in the treatment of hepatic encephalopathy. *Ther Clin Risk Manag*, 5, 617–626.
- Alvarez-Buylla, A., Ling, C.-Y., & Kirn, J. R. (1990). Cresyl violet: A red fluorescent Nissl stain. *J Neurosci Methods*, 33, 129–133.
- Basile, A. S., & Mullen, K. D. (2009). Hepatic encephalopathy A2. In Larry R. Squire (Ed.), *Encyclopedia of neuroscience* (pp. 1087–1093). Oxford, England: Academic Press.
- Brunt, E. M. (2000). Grading and staging the histopathological lesions of chronic hepatitis: The Knodell histology activity index and beyond. *Hepatology*, 31, 241–246.
- Brusilow, S. W., Koehler, R. C., Traystman, R. J., & Cooper, A. J. L. (2010). Astrocyte glutamine synthetase: Importance in hyperammonemic syndromes and potential target for therapy. *Neurotherapeutics*, 7, 452–470.
- Butterworth, R. F., Norenberg, M., Felipo, V., Ferenci, P., Albrecht, J., Blei, T. A., & Members of ISHEN Commission on Experimental Models of HE. (2009). Experimental models of hepatic encephalopathy: ISHEN guidelines. *Liver Int*, 29, 783–788.
- Carter, M., & Shieh, J. (2015). Chapter 2—Animal behavior. In M. Carter & J. Shieh (Eds.), *Guide to research techniques in neuroscience* (2nd ed., pp. 39–71). San Diego, CA: Academic Press.
- Casper, D., Yaparalvi, U., Rempel, N., & Werner, P. (2000). Ibuprofen protects dopaminergic neurons against glutamate toxicity *in vitro*. *Neurosci Lett*, 289, 201–204.
- Cauli, O., Rodrigo, R., Piedrafita, B., Llansola, M., Mansouri, M. T., & Felipo, V. (2009). Neuroinflammation contributes to hypokinesia in rats with hepatic encephalopathy: Ibuprofen restores its motor activity. *J Neurosci Res*, 87, 1369–1374.
- Chen, J.-R., Wang, B.-N., Tseng, G.-F., Wang, Y.-J., Huang, Y.-S., & Wang, T.-J. (2014). Morphological changes of cortical pyramidal neurons in hepatic encephalopathy. *BMC Neurosci*, 15, 15.
- Ciećko-Michalska, I., Szczepanek, M., Słowik, A., & Mach, T. (2012). Pathogenesis of hepatic encephalopathy. *Gastroenterol Res Pract*, 2012. doi:10.1155/2012/642108

- Conrad, C. D., Galea, L. A. M., Kuroda, Y., & McEwen, B. S. (1996). Chronic stress impairs rat spatial memory on the Y maze, and this effect is blocked by tianeptine pretreatment. *Behav Neurosci*, *110*, 1321–1334.
- Dhanda, S., & Sandhir, R. (2015). Role of dopaminergic and serotonergic neurotransmitters in behavioral alterations observed in rodent model of hepatic encephalopathy. *Behav Brain Res*, *286*, 222–235.
- Dhanda, S., Sunkaria, A., Halder, A., & Sandhir, R. (2018). Mitochondrial dysfunctions contribute to energy deficits in rodent model of hepatic encephalopathy. *Metab Brain Dis*, *33*, 209–223.
- El Hiba, O., Abbaoui, A., & Gamrani, H. (2016). Parkinsonism in acute hepatic encephalopathy: Experimental evidence in rat. *Parkinsonism Relat Disord*, *22*, e126.
- Every-Palmer, S., & Howick, J. (2014). How evidence-based medicine is failing due to biased trials and selective publication. *J Eval Clin Pract*, *20*, 908–914.
- Felipo, V., Urios, A., Montesinos, E., Molina, I., Garcia-Torres, M. L., Civera, M., Del Olmo, J. A., Ortega, J., Martinez-Valls, J., Serra, M. A., Cassinello, N., Wassel, A., Jordá, E., & Montoliu, C. (2012). Contribution of hyperammonemia and inflammatory factors to cognitive impairment in minimal hepatic encephalopathy. *Metab Brain Dis*, *27*, 51–58.
- Ferenci, P., Lockwood, A., Mullen, K., Tarter, R., Weissenborn, K., & Blei, A. T. (2002). Hepatic encephalopathy—Definition, nomenclature, diagnosis, and quantification: Final report of the Working Party at the 11th World Congresses of Gastroenterology, Vienna, 1998. *Hepatology*, *35*, 716–721.
- Fischer, A. H., Jacobson, K. A., Rose, J., & Zeller, R. (2008). Hematoxylin and eosin staining of tissue and cell sections. *CSH Protoc*, *2008*, pdb.prot4986.
- Gálvez-Gastélum, F. J., Garcia-Bañuelos, J. J., Beas-Zárate, C., Segura-Flores, A., González, H., Chaparro-Huerta, V., Salazar-Montes, A., Sandoval-Rodríguez, A. S., Bueno-Topete, M., Lucano-Landeros, S., Medina-Preciado, D., Gonzalez-Garcia, I., & Armendáriz-Borunda, J. (2010). Combinatorial gene therapy induces regression of hepatic encephalopathy. *Gene Ther*, *18*, 88.
- Georgiev, P., Jochum, W., Heinrich, S., Jang, J., Nocito, A., Dahm, F., & Clavien, P. A. (2008). Characterization of time-related changes after experimental bile duct ligation. *Br J Surg*, *95*, 646–656.
- Gil, M. N., Choi, D. R., Yu, K. S., Jeong, J. H., Bak, D.-H., Kim, D.-K., Lee, N.-S., Lee, J.-H., Jeong, Y.-G., Na, C. S., Na, D. S., Ryu, K.-H., & Han, S. Y. (2016). *Rhus verniciflua* Stokes attenuates cholestatic liver cirrhosis-induced interstitial fibrosis via Smad3 down-regulation and Smad7 up-regulation. *Anat Cell Biol*, *49*, 189–198.
- Giménez-Garzó, C., Salhi, D., Urios, A., Ruíz-Sauri, A., Carda, C., Montoliu, C., & Felipo, V. (2015). Rats with mild bile duct ligation show hepatic encephalopathy with cognitive and motor impairment in the absence of cirrhosis: Effects of alcohol ingestion. *Neurochem Res*, *40*, 230–240.
- Graham, L., & Orenstein, J. M. (2007). Processing tissue and cells for transmission electron microscopy in diagnostic pathology and research. *Nat Protocols*, *2*, 2439.
- Gyulkhandanyan, A. V., Mutlu, A., Freedman, J., & Leytin, V. (2015). Mitochondrial permeability transition pore (MPTP)-dependent and-independent pathways of mitochondrial membrane depolarization, cell shrinkage and microparticle formation during platelet apoptosis. *Br J Haematol*, *169*, 142–145.
- Hannan, E. L. (2008). Randomized clinical trials and observational studies: Guidelines for assessing respective strengths and limitations. *JACC Cardiovasc Interv*, *1*, 211–217.
- Izumi, Y., Yamamoto, N., Matsuo, T., Wakita, S., Takeuchi, H., Kume, T., Katsuki, H., Sawada, H. and Akaike, A. (2009). Vulnerability to glutamate toxicity of dopaminergic neurons is dependent on endogenous dopamine and MAPK activation. *J Neurochem*, *110*, 745–755.
- Jiang, X., & Wang, X. (2000). Cytochrome c promotes caspase-9 activation by inducing nucleotide binding to Apaf-1. *J Biol Chem*, *275*, 31199–31203.
- Jones, E., & Weissenborn, K. (1997). Neurology and the liver. *J Neurol Neurosurg Psychiatry*, *63*, 279–293.
- Kikuchi, S., & Kim, S. (1993). Glutamate neurotoxicity in mesencephalic dopaminergic neurons in culture. *J Neuroscience Res*, *36*, 558–569.
- Krishna, M. (2013). Role of special stains in diagnostic liver pathology. *Clin Liver Dis*, *2*, S8–S10.
- Lax, N. Z., Gorman, G. S., & Turnbull, D. M. (2017). Review: Central nervous system involvement in mitochondrial disease. *Neuropath Appl Neurobiol*, *43*, 102–118.
- Liu, A., Yoo, E. R., Siddique, O., Perumpail, R. B., Cholankeril, G., & Ahmed, A. (2017). Hepatic encephalopathy: What the multidisciplinary team can do. *J Multidiscip Healthc*, *10*, 113–119.
- Maddison, J. E. (1992). Hepatic encephalopathy: Current concepts of the pathogenesis. *J Vet Internal Med*, *6*, 341–353.
- Manning, R. T., & Delp, M. (1958). Management of hepatocerebral intoxication. *N Engl J Med*, *258*, 55–62.
- Mina Shaker, M., & Carey, W. D. (2014). *Hepatic encephalopathy*. Cleveland, OH: Cleveland Clinic
- Montagnese, S., Amodio, P., & Morgan, M. Y. (2004). Methods for diagnosing hepatic encephalopathy in patients with cirrhosis: A multidimensional approach. *Metab Brain Dis*, *19*, 281–312.
- Nabi, E., & Bajaj, J. S. (2014). Useful tests for hepatic encephalopathy in clinical practice. *Curr Gastroenterol Rep*, *16*, 362–362.
- National Research Council. (2010). *Guide for the care and use of laboratory animals*. Washington, DC: National Academies Press.
- Niknahad, H., Jamshidzadeh, A., Heidari, R., Zarei, M., & Ommati, M. M. (2017). Ammonia-induced mitochondrial dysfunction and energy metabolism disturbances in isolated brain and liver mitochondria, and the effect of taurine administration: Relevance to hepatic encephalopathy treatment. *Clin Exp Hepatol*, *3*, 141–151.
- Nojimoto, F. D., Mueller, A., Hebler-Barbosa, F., Akinaga, J., Lima, V., Kiguti, L. R., & Pupo, A. S. (2010). The tricyclic antidepressants amitriptyline, nortriptyline and imipramine are weak antagonists of human and rat alpha1B-adrenoceptors. *Neuropharmacology*, *59*, 49–57.

- Norenberg, M. D. (1987). The role of astrocytes in hepatic encephalopathy. *Neurochem Pathol*, *6*, 13–33.
- Norenberg, M. D. (1998). Astroglial dysfunction in hepatic encephalopathy. *Metabolic Brain Dis*, *13*, 319–335.
- Precht, T. A., Phelps, R. A., Linseman, D. A., Butts, B. D., Le, S. S., Laessig, T. A., Bouchard, R. J., & Heidenreich, K. A. (2005). The permeability transition pore triggers Bax translocation to mitochondria during neuronal apoptosis. *Cell Death Differ*, *12*, 255.
- Rao, K.V. R., & Norenberg, M. D. (2012). Brain energy metabolism and mitochondrial dysfunction in acute and chronic hepatic encephalopathy. *Neurochem Int*, *60*, 697–706.
- Rao, K.V. R., & Norenberg, M. D. (2014). Glutamine in the pathogenesis of hepatic encephalopathy: The trojan horse hypothesis revisited. *Neurochem Res*, *39*, 593–598.
- Rodrigo, R., Cauli, O., Gomez-Pinedo, U., Agusti, A., Hernandez-Rabaza, V., Garcia-Verdugo, J. M., & Felipo, V. (2010). Hyperammonemia induces neuroinflammation that contributes to cognitive impairment in rats with hepatic encephalopathy. *Gastroenterology*, *139*, 675–684.
- Romero-Gómez, M., Montagnese, S., & Jalan, R. (2015). Hepatic encephalopathy in patients with acute decompensation of cirrhosis and acute-on-chronic liver failure. *J Hepatol*, *62*, 437–447.
- Ruiz-Meana, M., Abellán, A., Miró-Casas, E., & Garcia-Dorado, D. (2007). Opening of mitochondrial permeability transition pore induces hypercontracture in Ca²⁺ overloaded cardiac myocytes. *Basic Res Cardiol*, *102*, 542.
- Shiotsuki, H., Yoshimi, K., Shimo, Y., Funayama, M., Takamatsu, Y., Ikeda, K., Takahashi, R., Kitazawa, S., & Hattori, N. (2010). A rotarod test for evaluation of motor skill learning. *J Neurosci Methods*, *189*, 180–185.
- Stavrovskaya, I. G., Narayanan, M. V., Zhang, W., Krasnikov, B. F., Heemskerk, J., Young, S. S., Blass, J. P., Brown, A. M., Beal, M. F., Friedlander, R. M., & Kristal, B. S. (2004). Clinically approved heterocyclics act on a mitochondrial target and reduce stroke-induced pathology. *J Exp Med*, *200*, 211–222.
- Stockert, J. C., Blázquez-Castro, A., Cañete, M., Horobin, R. W., & Villanueva, Á. (2012). MTT assay for cell viability: Intracellular localization of the formazan product is in lipid droplets. *Acta Histochem*, *114*, 785–796.
- Swaminathan, M., Ellul, M. A., & Cross, T. J. S. (2018). Hepatic encephalopathy: Current challenges and future prospects. *Hepat Med*, *10*, 1–11.
- Tag, C. G., Sauer-Lehnen, S., Weiskirchen, S., Borkham-Kamphorst, E., Tolba, R. H., Tacke, F., & Weiskirchen, R. (2015). Bile duct ligation in mice: Induction of inflammatory liver injury and fibrosis by obstructive cholestasis. *J Vis Exp*. doi:10.3791/52438
- Takano, H., Arakawa, R., Nogami, T., Suzuki, M., Nagashima, T., Fujiwara, H., Kimura, Y., Kodaka, F., Takahata, K., Shimada, H., Murakami, Y., Tateno, A., Yamada, M., Ito, H., Kawamura, K., Zhang, M. R., Takahashi, H., Kato, M., Okubo, Y., Suhara, T. (2014). Norepinephrine transporter occupancy by nortriptyline in patients with depression: A positron emission tomography study with (S,S)-[¹⁸F]FMeNER-D₂. *Int J Neuropsychopharmacol*, *17*, 553–560.
- Tatem, K. S., Quinn, J. L., Phadke, A., Yu, Q., Gordish-Dressman, H., & Nagaraju, K. (2014). Behavioral and locomotor measurements using an open field activity monitoring system for skeletal muscle diseases. *J Vis Exp*, *91*, 51785.
- Wang, H., Guan, Y., Wang, X., Smith, K., Cormier, K., Zhu, S., Stavrovskaya, I. G., Huo, C., Ferrante, R. J., Kristal, B. S., & Friedlander, R. M. (2007). Nortriptyline delays disease onset in models of chronic neurodegeneration. *Eur J Neurosci*, *26*, 633–641.
- Watford, M. (2003). The urea cycle: Teaching intermediary metabolism in a physiological setting. *Biochem Mol Biol Educ*, *31*, 289–297.
- Yamada, A., Takeuchi, H., Miki, H., Touge, T., & Nishioka, M. (1992). Decreased dopaminergic activity in hepatic encephalopathy in rats with galactosamine-induced acute liver failure. *No To Shinkei*, *44*, 103–109.
- Zhang, W.-H., Wang, H., Wang, X., Narayanan, M.V., Stavrovskaya, I. G., Kristal, B. S., & Friedlander, R. M. (2008). Nortriptyline protects mitochondria and reduces cerebral ischemia/hypoxia injury. *Stroke*, *39*, 455–462.